5

Mixing and Segregation

5.1. Introduction

Liquids have a well-known predisposition for miscibility.[1] Dry granular materials, by contrast, are notorious for being difficult to mix homogeneously.[2] Two granular materials differing by their density, shape, size, or even by their micromechanical properties (such as coefficient of elastic restitution and friction), exhibit a distinct propensity for segregation. This phenomenon is a fundamental property of the granular state and an unending source of frustration in industry. Whenever a mixture undergoes a flow, a vibration, or a shearing action, the components tend to separate partially or completely, depending on the circumstances. By analogy with chemical reactions, we may say that under the influence of various stimuli a granular mixture inexorably tends to self-organize so as to locally reconstruct clusters of identical particles.

As we have pointed out in the Introduction to this book, the segregation of dry granular materials can be routinely observed even in the most primitive table-top

[1]Since liquids are made of particles subject to Brownian motion, thermal agitation alone produces mixing. As pointed out in Chapter 1, the Brownian motion of granular particles is entirely negligible. Another source of energy is then required to achieve mixing. Vibration is a logical candidate, even though the final result is often the exact opposite of what is being sought!

[2]The concept of "homogeneous mixture" needs to be clarified in a granular material. A mixture composed of a fraction α of granules A and β of granules B (with $\alpha+\beta=1$) is said to be homogeneous on a scale λ if a volume λ^3 contains the two ingredients in the right proportions. We can appreciate that optimum homogeneity will be achieved when the smallest scale λ, for which the mixture can still be considered homogeneous in the sense just defined, is of the order of the size of the largest of the two types of particle.

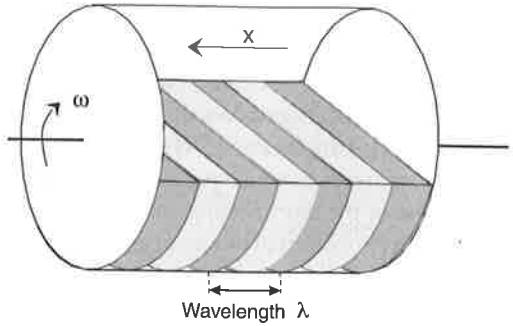

FIGURE 96. Oyama's horizontal drum rotates around its axis. An initially homogenous granular mixture segregates in vertical bands with a spatial periodicity λ.

experiments by shaking a mixture of different grains (wheat, corn, rice, salt, are all good candidates) in a test tube.[3] Likewise, farmers know very well that tilling fields causes large rocks, in seemingly endless supply, to work their way up to the surface. Peasants in India take advantage of the segregation properties of dry granulars by shaking their harvest of chickpeas in baskets in order to separate them from other materials. When Brazil nuts, mixed with other smaller nuts, are transported in pick-up trucks over the rough back roads of South America, they invariably end up on top of the load.[4] In short, the phenomenon of segregation in dry granulars is universally recognized, even though it may not be well understood.

The first recorded observation of segregation in a three-dimensional medium was described by Oyama in 1939.

5.1.1. Oyama's Cylindrical Drum

Oyama's experiment is schematically illustrated in Figure 96 [89]. It consists in mixing two granulars of the same type but of different sizes and colors. For instance, we may use glass beads, some of which are transparent and 500 μm in diameter, while the others are dark-colored and 100 μm in diameter. They are mixed in equal volumes and placed in an elongated cylindrical container which is rotated horizontally around its axis.

As Oyama reported, the large and small beads divide themselves in vertical strata, as depicted in Figure 96. The process starts with just a few slow rotations of the drum. After a sufficiently long time, the segregation continues, first into three, and then five zones typically observed after about an hour. The phenomenon takes place only when the rotation speed is rather slow, although nobody really

[3]The importance of using *dry* materials cannot be overemphasized. It is essential that any interaction with the ambient fluid be negligible. If not, the problems are of a radically different nature. Well-designed cement trucks, for instance, are perfectly capable of adequately mixing gravel of various sizes with cement and water.

[4]The example of Brazil nuts has become a paragon in matters of granular segregation following the publication in *Physical Review Letters* of a paper entitled "Why do Brazil nuts are on top?". To speak of "Brazil nut" phenomenon has become synonymous with the problem of segregation by size.

knows why. Spectacular as it may be, this experiment remains poorly understood. It continues to be the object of numerous studies, some of which rely on sophisticated techniques such as nuclear magnetic resonance (see Section 3.2.3) [90].

Be that as it may, the experiment underscores the amazing efficacy of segregation by rotation or, to be more precise, by shearing. As mentioned earlier, segregation is a very general property of mixtures in which particles are in motion relative to one other. A careful observation of the mechanisms potentially involved has led some authors to distinguish at least two different modes of granular segregation. They are:

- *Segregation by Vibration*. The relative motion of the particles is imparted by shaking the container—usually in a vertical direction. When the situation involves small particles in the midst of larger ones, we may further distinguish segregation by convection, by arch effects, and by percolation.
- *Segregation by Shearing*. Here, segregation is caused by a differential flow of overlaid sheets, in the manner described in Section 2.4.2. A useful picture is that of a bulldozer churning large rocks to the surface of the ground, as is commonly observed in earth-moving projects.

Given our limited understanding of this phenomenon, it is important to acknowledge that the details of the mechanisms at play remain for the most part a mystery. No one has a handle on the fundamental laws governing the segregation of objects with different densities or masses, or with different mechanical coefficients. That goes both for segregation by vibration and by shearing. Likewise, very little is known about the segregation of objects of different sizes, except perhaps in the context of a few simulations of the type to be discussed in Chapter 6. For reasons that are quite easy to understand, most researchers currently working on this problem have limited themselves—at least up to now—*to segregation by size*. That is in fact, the primary topic covered in this chapter. As we are about to see, even this issue turns out to be anything but trivial. In a first step, we will restrict our focus to the segregation of a single particle differing in size from all the other particles that constitute its environment. The purpose of this step-by-step approach is to hopefully extract the fundamental laws governing the physics of the process. It appears to be a general property of granular materials to want to expel the largest objects out toward the periphery. For instance, shaking a granular medium causes large particles to migrate toward the top of a pile.

5.1.2. *Potential Energy of a Heterogeneous Pile*

Before attacking more specifically the mechanism of demixing in vibrated or sheared granulars, it is important to realize, starting from elementary considerations of the energy of heterogeneous piles, that segregation by size is indeed a phenomenon characteristic of these materials. As it turns out, this property can be understood as a consequence of Reynolds's dilatancy principle, consistent with arguments developed in Section 3.1.3.

We begin with a few general observations about stacks of spheres (in three dimensions) or of cylinders (in two dimensions). Consider two spheres of masses

M and m, and radii R and r (with $M > m$ and $R > r$), stacked on top of each other. If the large sphere is on top, the potential energy E_p of the stack can be written as

$$E_p = mgr + Mg(R + 2r),$$

where the horizontal base on which the edifice rests is taken as reference. Both spheres are assumed to be made of the same material and, therefore, have the same volumetric density. This additional piece of information leads to an expression for the potential energy in terms of sizes only

$$E_p \propto r^4 + R^4 + 2rR^3.$$

Interestingly, this expression is not symmetrical in r and R, which means that the energy depends on whether the large or the small sphere is on top. Not surprisingly, the configuration with the small sphere on top is energetically favorable. We may find a degree of solace in this result. Yet, our intuition clearly fails us when it comes to the phenomenon of segregation by size which, as already indicated, invariably drives the largest—hence, heaviest—particles toward the top.

Superposition of Stacks—Two Compact Stacks

We next consider the stack shown in Figure 97. The structure, depicted here in two dimensions, is made of two kinds of marble made of the same material. The marbles differ only by their diameter and are arranged in two zones stacked in a compact triangular lattice (which gives it maximum compactness, in accordance with Section 3.1.3). They are placed in a cylindrical container of cross-sectional area S. We designate by V and v, respectively, the volumes of each of the zones occupied by marbles of radii R and r. Assuming that the largest marbles occupy

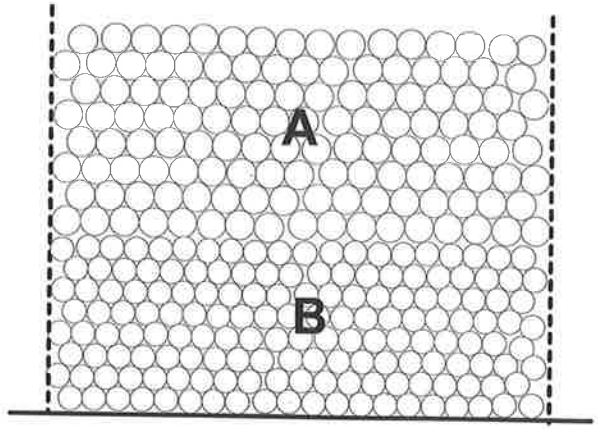

FIGURE 97. Two types of particles A and B of different sizes are stacked in superposed layers. In the absence of any structural defect, A/B and B/A configurations are equivalent from an energy point of view.

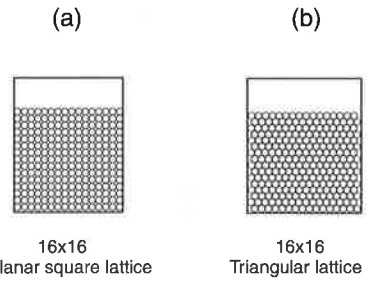

FIGURE 98. Two stacking modes for two-dimensional structures. The triangular configuration (b), being as compact as possible, has a lower potential energy than configuration (a). It is therefore energetically favorable and more stable.

the upper part of the container, the potential energy of the entire pile is given by

$$E_p \propto \frac{v^2}{2} + \left(v + \frac{V}{2}\right)V \propto (v+V)^2.$$

This time, which type of marble is on top has no bearing from an energy point of view, and there is no reason to anticipate any segregation, at least as long as interface effects are absent. This result is obvious, inasmuch as two layers of identical density are always in equilibrium.

Without the benefit of a more detailed analysis, we may begin to suspect that structural defects in a lattice made of particles of different sizes may have something to do with the tendency of large particles to work their way back up. To explore this possibility, we return to two configurations already discussed in Section 3.1.3. The relevant structures are reproduced in Figure 98.

An elementary analysis of the two stacks shows that the triangular lattice is—based on simple energy arguments—more probable and stable than its square counterpart. As we have seen, the compact triangular lattice is the only one to exhibit characteristics consistent with Reynolds's dilatancy principle. The reader will recall that a compact stack subjected to any distortion can only respond by expanding, which increases its potential energy. If we realize that distorting a compact triangular lattice necessarily entails the creation of defects in the stack, we may legitimately inquire whether such defects may tend to concentrate in the lower or the upper portion of the pile. In particular, what can energy arguments tell us about this question?

Where Are the Defects Concentrated?

We start from a structure made of identical spheres in a state of maximum compactness, and assume that a number of defects are somehow created either in the upper or in the lower region, both of which have the same volume v. Our intuition suggests that the energetically favorable situation is to have the defects near the top. We can verify this by calculating the potential energy in both cases. The potential

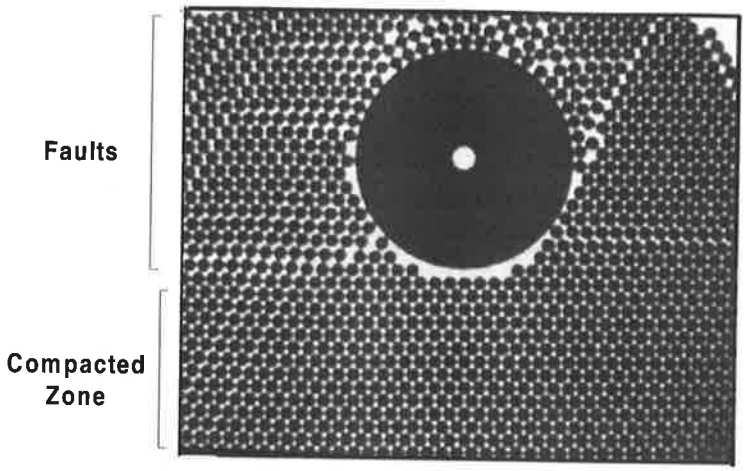

FIGURE 99. Defects are created when a large disk is inserted into a two-dimensional stack. The photograph was obtained by back-illuminating a real stack. The lower part of the stack remains compacted, while the triangular symmetry of the upper part is greatly disturbed by the introduction of the large disk (after [93]).

energy is denoted E_{pu} if the defects are in the upper region, and E_{pl} otherwise. If the defects involve an increase in volume dv, the calculation indicates that

$$E_{pl} - E_{pu} \propto v\,dv > 0,$$

which implies that defects near the top are indeed energetically preferred. Another way to express the same result is that, in a cylindrical container, the potential energy is minimum when the less dense material is on top.

An equivalent two-dimensional experimental configuration, similar to those we have discussed in Chapter 3, is easy to implement with suitable provisions for agitation.[5] All we need to do is to introduce into the container a single larger disk of the same volumetric density as the rest of the pile, and we can readily witness the phenomenon just described. As demonstrated in Figure 99, the intruder causes local distortions in the lattice by creating defects which tend to migrate to the upper part of the structure.[6]

When viewed in this context, the process of segregation by size emerges as one of the consequences of the dilatancy principle. The introduction of an intruder necessarily causes a local distortion of the lattice manifesting itself in a local expansion. The expanded and, therefore, less dense portion of the pile tends to

[5]The meaning of the phrase "suitable agitation" deserves to be thought out carefully. It may be said that shaking (or vibrating) a complex granular edifice enables us to explore perhaps not all but at least many of the possible configurations of a pile. Several simulation approaches (notably the Monte Carlo technique, to be discussed in Chapter 6) capitalize on this observation by minimizing the energy after each perturbational event through various relaxation processes.

[6]We will often use the term "intruder" to refer to a particle whose size or other properties differ from those of the "normal" sea of particles which, for the sake of simplicity, we will consider uniform.

move toward the top, dragging the intruder along with it. This would suggest that the shape of the intruder may play a crucial role in the process of segregation, depending on how readily it may fit in the surrounding lattice.

There are too many potential objections to accept such a crude explanation at face value. In an attempt to get a better grasp of the phenomenon, we will have to refine our understanding of the successive relaxation states of a pile undergoing segregation. Until then, the one idea that should stand out and be remembered in what follows is that size segregation implies defects created by the intruder in its environment.

5.2. Segregation by Vibration

As pointed out on several occasions already, shaking or vibrating a mixture of particles for the purpose of studying the process of segregation is a most efficient and reliable method. It is routinely used both in industry and in the laboratory. Indeed, vibrating a collection of particles is the best way to explore systematically a large number of possible configurations. We might add that this mode of excitation lends itself readily to numerical computer simulations, an advantage that is not to be overlooked. The frequency and amplitude of the vibrations are easy to control, and a typical experiment boils down to following what happens to a large and clearly marked particle in its environment. By adding a few tracers to the matrix, we can even get a fairly clear picture of how the surrounding particles move about.

5.2.1. Simulation of Segregation by Size

Before proposing a model that can account for the behavior of a vibrated two-dimensional pile composed of a single intruder in an otherwise homogeneous environment, it is useful to pause and consider Figure 100, as it highlights a number of remarkable characteristics of such structures.

For starters, we note that both computer-generated and real-life stacks feature stacking faults in the form of distortions and dislocations in the upper part of the structure. This is fully consistent with our previous elementary energy considerations. In addition, we see that the perturbation caused by an intruder whose size is different from that of the particles composing the matrix develops in an essentially triangular pattern. We might think that this pattern is simply a consequence of the symmetry characteristic of the type of two-dimensional lattice considered here. However, as we shall soon see, this property is not restricted to two-dimensional lattices. Computers can serve as an inexhaustible source of synthetic three-dimensional piles, whose geometry can be easily studied [91]. It turns out that, in this case too, defects are generated in the upper part of the pile, and their geometry is quite similar to what is observed in two dimensions. That provides confidence for extending the arguments we are about to develop to three-dimensional piles.

Lastly—and this is crucial for the model discussed next—we can see that a large-size intruder, such as in Figures 100(a) and (c), does not necessarily have to

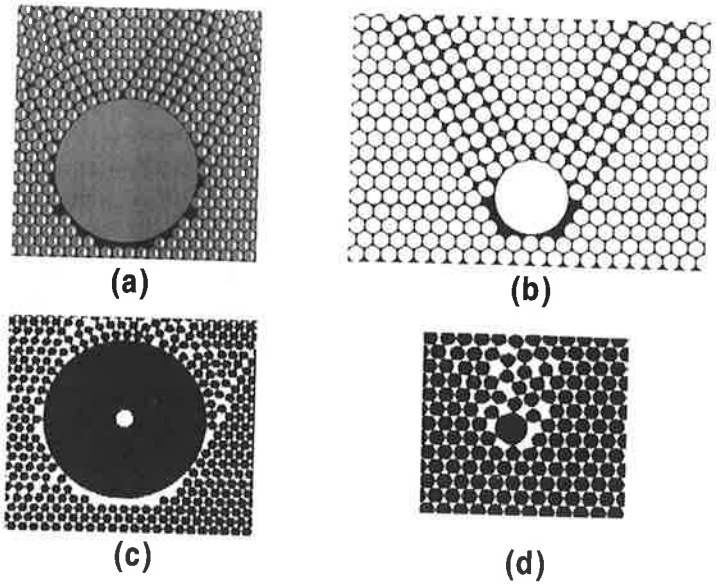

FIGURE 100. Different configurations of a two-dimensional inhomogeneous stack. Diagrams (a) and (b) are computer-generated structures, while (c) and (d) are photographs of actual real-life stacks. Note that a large intruder can be in a stable position without having to be in contact with particles immediately below (arch effect) (after [93]).

rest on lattice lines associated with the matrix. Instead, they can be propped up above such lines by lateral particles, somewhat like the arch of a cathedral rests on stones that transmit its weight to side columns. Pursuing this metaphor, we refer to this phenomenon as the *arch effect* or *vault effect*.

When trying to model the dynamic properties of such a system, we need to inventory all possible stable positions of the intruder. Stability occurs under one of two conditions:

- The intruder rests on a lattice line defined by the ordered arrangement of spheres constituting the environment.
- The intruder is kept above a lattice line because it sticks at two points marked by arrows in Figure 101. The line formed by joining these two points traverses the intruder below its center of gravity. Should that process fail, the intruder drops back down to the next lowest lattice line.

Modeling this situation involves solving a topological problem, which goes something as follows: The intruder is raised a very small step at a time, as depicted in Figure 102, and the system is left to reorganize itself by relaxing around the intruder. The new arrangement is examined to determine if it is stable or unstable. If it is unstable, the intruder is raised some more by a tiny amount, and the stability is examined again. The process makes it possible to find eventually all stable configurations.

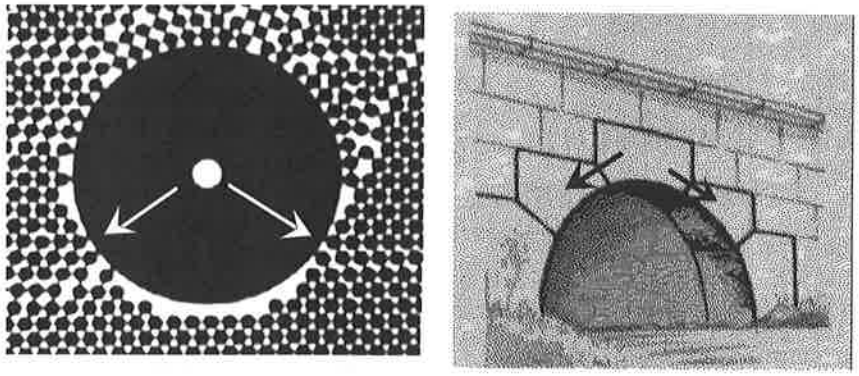

FIGURE 101. Simulation of the equilibrium of an intruder by the arch effect. On the left is a photograph of an actual stack of metal spheres containing a foreign disk (after [93]).

Two-Dimensional Model

The relevant geometry is illustrated in Figure 103(a). Let $\Phi = R/r$ be the ratio (> 1) of the radii of the particles. As indicated earlier, the effective part of the pile is confined within walls $B_1(T)$ and $B_2(T)$, which in the present case intersect at an angle of 60°. Our purpose is to determine all stable positions of the intruder as it is being raised in a step-by-step fashion up the pile. The first thing we notice is that, because of the geometry of the structure, we do not have to explore a height greater than one period of the structure, which is given by $\Theta = 2r\sqrt{3}$, or 3.46 times the radius of the dominant particles. Let h be the altitude of the intruder's center, as shown in Figure 103(a). We keep track of each particle by its row (index i) and column (index j). Simple geometry considerations show that the stable positions

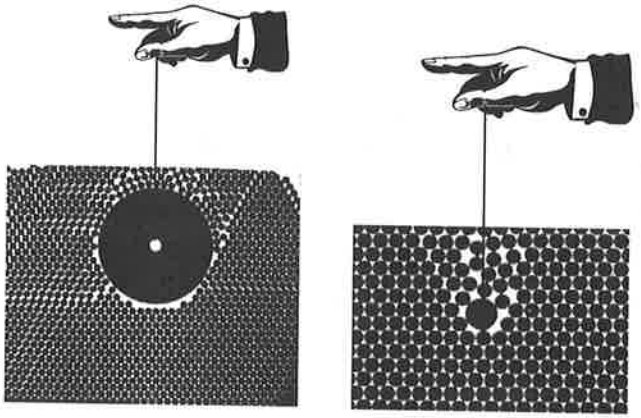

FIGURE 102. Method for seeking the equilibrium positions in a stack by exploring different possible configurations.

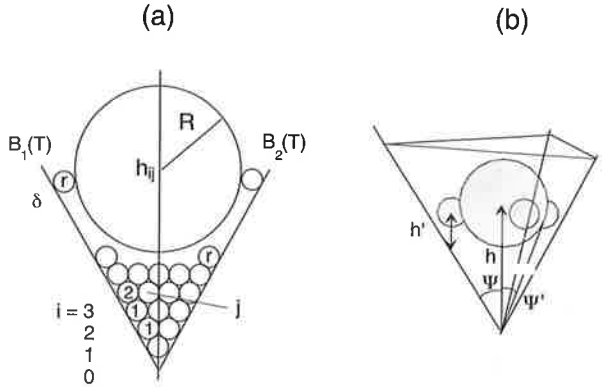

FIGURE 103. Diagrams of two- and three-dimensional stacks used to develop a model of segregation by the arch effect.

of the intruder, i.e., when it rests on a lattice line, are obtained when

$$h_{ij}^{S} = [(R+r)^2 - r(2j-k)^2]^{1/2} + 2r\left(1 + i\frac{\sqrt{3}}{2}\right),$$

where the superscript S indicates that the position is stable. The index k runs from $[(-1)^{i+1}+1]/2$ to $\mathrm{Int}((i+1)/2)$, the operator $\mathrm{Int}(m)$ designating the nearest truncated integer of the argument m.

Next we look for stable positions of the intruder via vault effects, that is to say, when it rests on two particles located below its center of gravity. We start from a situation where the intruder is in contact with the two lateral walls $B_1(T)$ and $B_2(T)$, which occurs when $h^{v1} = 2r$. When the intruder is raised gradually, it will find a new stable position when two small particles can just squeeze below its center of gravity. This happens when $h^{v2} = (R+\delta)\sqrt{3} \approx r\sqrt{3}(\Phi+2)$, where δ is the space between the intruder and the lateral walls.[7] The fraction S of stable vault configurations over a period Θ is given by

$$S = 1 - \frac{h^{v2} - h^{v1}}{\Theta} = \frac{2-\sqrt{3}}{2\sqrt{3}}\Phi \approx 0.077\,\Phi.$$

A smooth rise through a *continuum* of vault configurations is obtained when $S = 1$, which happens when $\Phi_c^{2D} \approx 12.9$. As such, the quantity Φ_c^{2D} can be construed as a *critical ratio of diameters* marking the boundary between two types of behavior [92], [93]. On one side of the dividing line, the intruder rises continuously, while on the other it goes through a series of discrete steps determined by the size of the smaller particles. This line of reasoning makes it possible to calculate analytically,

[7] In this approximation, we assume $\delta \approx 2r$. The exact solution would require lining the boundary with small particles. The walls would then no longer be straight but made of a succession of connected half-circles. The approximation is justified a posteriori by numerical simulations.

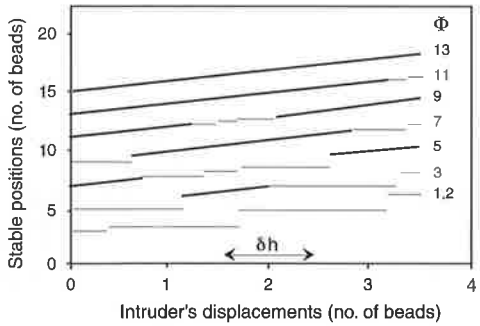

FIGURE 104. Ascension diagram of an intruder of radius Φr in a matrix of particles of radius r. The thick solid lines indicate the stable positions of the intruder as it rises via the arch effect. The horizontal plateaus (fine solid lines) correspond to a discrete series of positions in which the intruder rests on a lattice line of the matrix. The quantity δh denotes the small relative displacements of the intruder and the surrounding lattice.

or by means of simulations which will be discussed in Chapter 6, diagrams showing the intruder's stable positions plotted against its displacements. Figure 104 is an example of such a plot.

Three-Dimensional Model

It is relatively straightforward to extend the preceding model to the case of three dimensions. The triangle (T) becomes a tetrahedron which obeys the same symmetry. Using the notation indicated in Figure 103(b), we have

$$h - h' = \frac{R - r}{\sin \Psi} = \frac{R + r}{\tan \Psi'},$$

where $h = 3R$, $h' = 3r$, $\Psi = \cos^{-1}(\frac{1}{3})$, and $\Psi' = \tan^{-1}(\sqrt{2}/2)$.

The critical diameter for continuous rise via vault effects in three dimensions is given by

$$\Phi_c^{3D} = \frac{3 + \sqrt{2}}{3 - \sqrt{2}} \approx 2.78,$$

which turns out to be remarkably close to values found by numerical simulations, which will be covered in Chapter 6 [91].

5.2.2. *Experiments on Segregation by Vibration*

The first quantitative experiments aimed at studying the phenomenon of segregation by size were begun only in the late 1970s. For lack of a better technique, the experimental approach consisted simply in measuring the time taken by an intruder placed at the bottom of a container filled with a granular material to make its way back up to the surface when subjected to vibrations [94]. This method was much too primitive to reveal the subtleties of granular segregation which we are

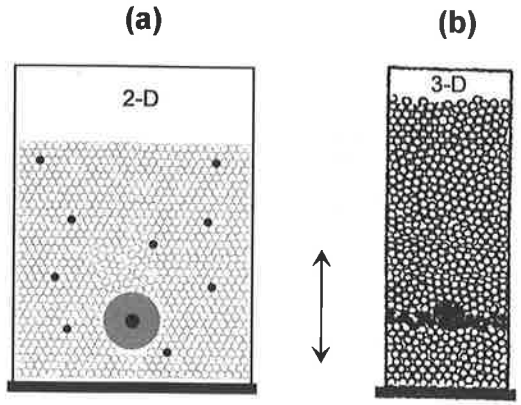

FIGURE 105. Diagram of experimental methods used to study the segregation by shaking of a large particle in either (a) two-dimensions or (b) three-dimensions. In (a), a large marked intruder is immersed in a population that includes a few tracers (black particles), whose progression is tracked by image processing techniques. In (b), the movement of tracer particles in their environment is monitored by direct visual observation.

Modern techniques take advantage of the possibilities offered by image processing (see Section 3.2.3), as well as nuclear magnetic resonance, which makes it possible to monitor what goes on inside a three-dimensional opaque system. More direct methods rely on suitably prepared samples containing tracer particles. The technique, schematically illustrated in Figure 105, has been used to study both two- and three-dimensional configurations [93], [95].

A typical implementation of the approach is shown in the photograph of Figure 106. The apparatus uses two small cameras. The first, placed next to a vibrating

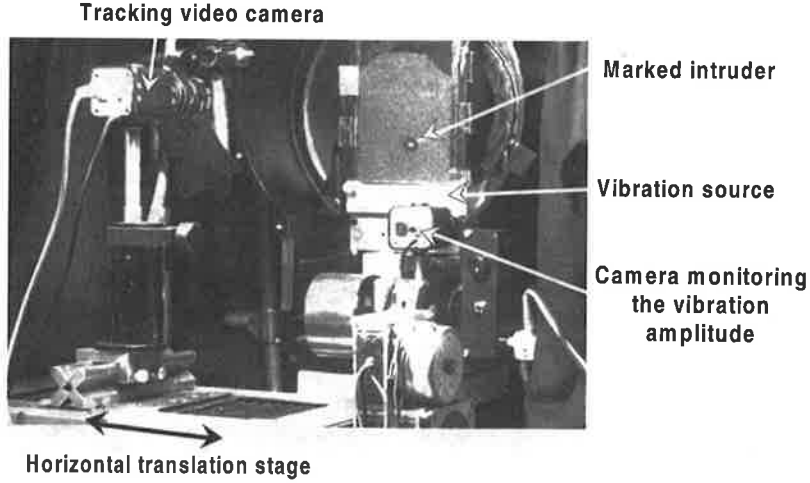

FIGURE 106. Photograph of an experimental setup designed to track the ascending move-

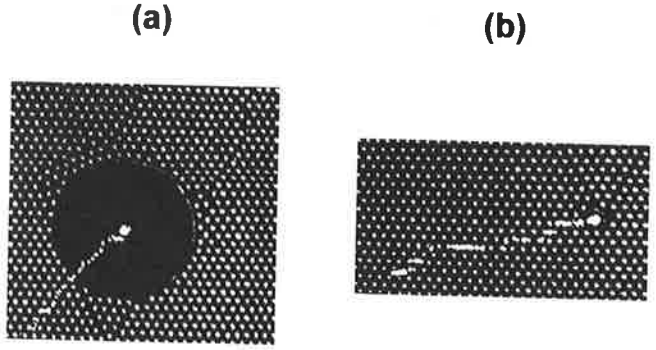

FIGURE 107. Experimental observations of the movement of an intruder. Diagram (a) corresponds to a continuous rise ($\Phi = 16$ and $\Gamma = 1.2$), while (b) reveals successive plateaus ($\Phi = 2$ and $\Gamma = 1.4$). The doted white line in (a) is an artifact due to the image processing technique. It is quite real, on the other hand, in (b), which was generated by directly displaying the height of the moving object as a function of time. The horizontal scale corresponds to about 1 hour (after [93]).

plate, measures accurately the amplitude of the vibration. The second is mounted on a translation stage and connected to the image processing electronics. With thresholding and the image addition techniques described in Section 3.2.3, it is possible to track one or more particles during the course of an experiment.[8] Alternatively, by moving the camera horizontally at constant speed, the vertical position $h(t)$ of the intruder can be displayed directly on the monitor's screen as a function of time. We will see several examples of this technique below.

Experiments on Continuous and Intermittent Ascent

An apparatus similar to the one just described has been used to study the different modes of ascent of cylindrical disks of various sizes immersed in a uniform granular medium. Experiments show that a small intruder "sees" the discontinuities of the granular environment, which is to be expected. A large disk, on the other hand, rises smoothly without any pauses, which is not at all intuitive. Disks of intermediate sizes exhibit continuous rises interspersed by plateaus, in agreement with the predictions of the ascent diagram.

The model does seem to predict fairly well whether an intruder will ascend continuously (Figure 107(a)) or intermittently (Figure 107(b)). On the other hand, it tells us nothing about what *causes* the ascent in the first place. A careful observation of the vibrated container offers some hints as to what drives the intruder toward the top.

With the aid of a suitable stroboscopic lighting system, it is easy to observe fractures with various lifetimes appearing in the immediate vicinity of the intruder, as shown in Figure 108.

[8] "Thresholding" consists in defining a particular level of brightness. Anything brighter than that level is considered white (or 1), and anything darker becomes black (or 0).

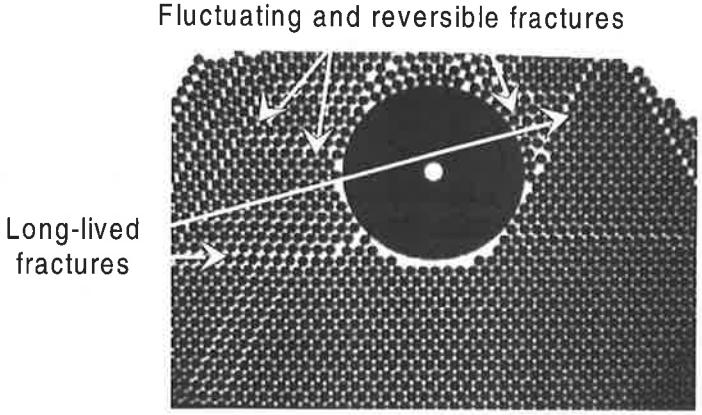

FIGURE 108. Photograph showing the relatively random appearance of fractures around the intruder (after [93]).

Referring to the ascent diagram of Figure 104, we can make the following observations:

- A small intruder (one that is characterized by $\Phi < 12.9$) requires a large relative displacement δ between itself and its environment in order to overcome each step in the ascent diagram. Accordingly, we may anticipate a sizable vibration threshold to initiate this kind of motion. Experiments indeed confirm this.
- A large intruder (one with $\Phi > 12.9$) proceeds much more readily while remaining continuously in an arch configuration. We can predict—and it is experimentally verified—that the amplitude threshold is much lower than in the previous case. In other words, a larger intruder moves up far more easily than a small one.

As we will see, this is further confirmed by diagrams of upward speed as a function of the ratio $\Phi = R/r$, at least on condition that we avoid the *convection regime*. In this respect, experiments that make it possible to observe simultaneously the upward drift of the intruder and the relative motions of the surrounding particles are highly revealing.

Finally, we might point out that the phenomena of continuous and discontinuous ascent just discussed have never been observed up to now in three dimensions, even though simulations predict them. That does not necessarily mean that they do not exist.

Convection or Arch Effect?

Experiments conducted in two or three dimensions show that, when the vibration is sufficiently intense, particles experience a phenomenon of convection similar to what we have already encountered in Chapter 3. We proceed to provide additional details pertinent to these two situations. We start with three-dimensional configurations.

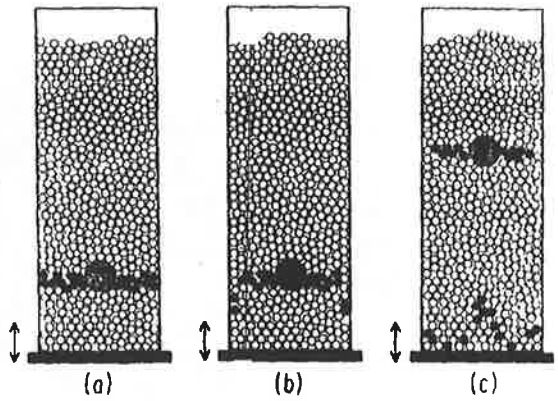

FIGURE 109. Schematic description of three-dimensional experiments on the segregation of a single intruder. Diagram (a) shows the initial configuration. In (b), the intruder has begun its ascent, while some small black tracers have started to move down along the lateral walls. Diagram (c) depicts the situation some time later, when convection recirculates the black particles dragged to the bottom along the sides, while a central convective flow pushes the intruder toward the top (after [95]).

Convection and Segregation in Three Dimensions

A series of experiments, conducted in a cylindrical container with and without an intruder (see Figure 54), demonstrated convincingly the existence of convection movements in a column of granular material subjected to energetic impulses separated by periods of the order of a second, so as to let the system relax back between successive excitations [95]. Figure 109 illustrates schematically the kinds of phenomena that are typically observed in such an experiment in the presence of an intruder.

The results shown in Figure 110 demonstrate that, regardless of the size of the intruder, its upward movement proceeds at the same speed as that of the convective flux of the matrix. For purely geometrical reasons, large intruders cannot return back down alongside the walls the way the main population of particles does. We may conclude that we are dealing here with segregation by pure convection. Segregation by convection takes place both in two- and three-dimensional configurations. It is very important to remember that when convection drives the process, the ascending speed does not depend on the size of the intruder, in marked contrast with the arch effect mechanism.[9]

Convection and Segregation in Two Dimensions

We now report the results of experiments conducted in two-dimensional cells of the type described earlier [97]. Figure 111 shows CPP photographs of a

[9]Some degree of caution is warranted in making this statement. It has not actually been proven that the intruder itself does not somehow induce convection. The dynamic maps presented in Figure 111 would suggest that such is not the case and that the intruder does not promote convection, at least not

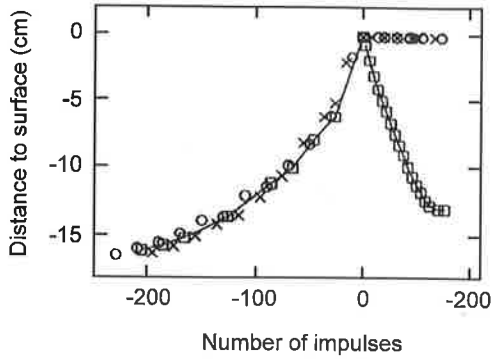

FIGURE 110. Successive positions of different intruders plotted against the number of impulsions applied to the container. The ratio Φ is equal to 9.5 (crosses), 6 (circles), and 1 (squares), respectively. Note that large intruders remain trapped at the surface after completing their climb, while small ones (square data points) are dragged back down to the bottom by convection (after [95]).

two-dimensional pile vibrated vertically with varying accelerations. Figure 111(a) reveals a process of convection identical to the one just discussed in three dimensions. By contrast, Figure 111(b) is indicative of an arch effect squeezing the intruder. As emphasized above, this phenomenon depends on the intruder's size. The velocity of the upward movement is presumably a function of the diameter ratio Φ. This was entirely confirmed by a set of experiments recording the altitude $h(t)$ of intruders of various sizes as a function of time for a given acceleration and container configuration. The results of these experiments are reproduced in Figure 112.

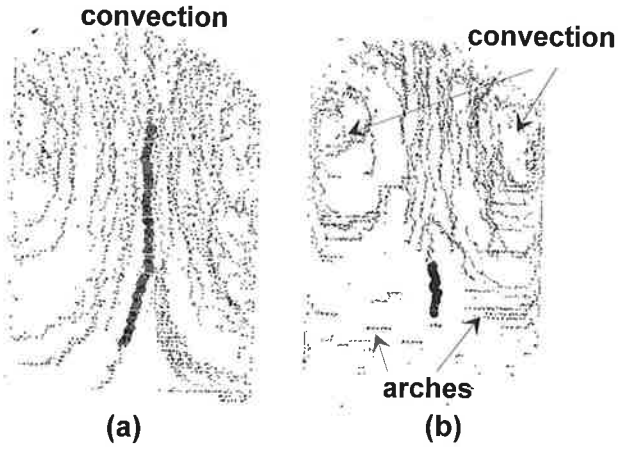

FIGURE 111. Diagram (a) shows a typical segregation mechanism by convection observed with a relatively strong excitation ($\Gamma = 1.6$). Diagram (b) was obtained with a weaker acceleration ($\Gamma = 1.2$). It reveals an arch effect mechanism that displaces markers laterally below the intruder. This latter mode of segregation acts differently on intruders of different

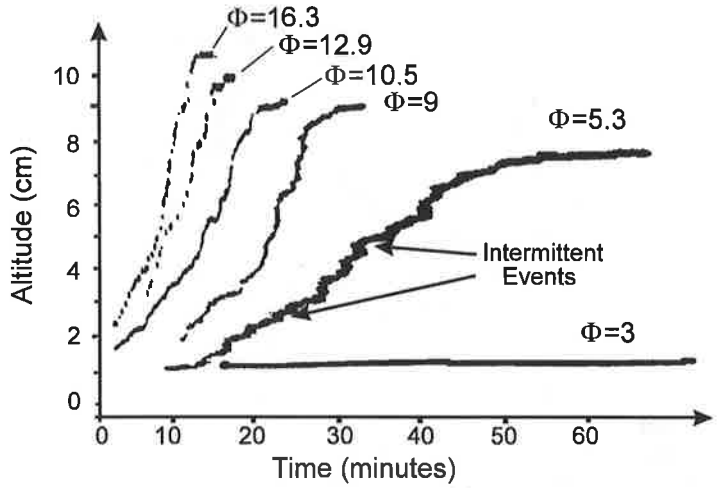

FIGURE 112. Positions $h(t)$ of intruders of various sizes immersed in a bath of particles 1.5 mm in diameter. The larger the size of the intruder, the faster its ascent (after [93]).

Here the acceleration was held constant at $\Gamma = 1.25$. The various curves $h(t)$ have been displaced along the horizontal axis to make it easier to tell them apart. The results clearly demonstrate a process of size segregation consistent with the arch effect model discussed earlier. Small-size intruders ($\Phi < 12.9$) experience a discontinuous ascending motion marked by a series of steps and plateaus. The greater the size of the intruder, the less discontinuous its upward movement, in agreement with the model. All of this is consistent with the ascent diagram shown in Figure 104. Furthermore, with small enough intruders (characterized by $\Phi < 3$), no ascending movement occurs at all, at least not for this particular acceleration and over the duration of the experiment (about 1 hour). The results, summarized in Figure 113, prove that there is indeed a threshold diameter below which any

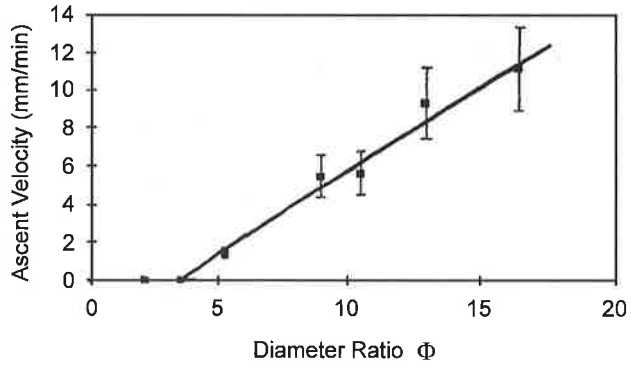

FIGURE 113. Ascending velocity measured from Figure 112 as a function of the diameter ratio Φ (after [93]).

ascending motion is inhibited. The existence of the threshold diameter makes sense on the basis of the ascent diagram in Figure 104. We noted at the time that, for weak accelerations, the fluctuations δh of the intruder's positions can be smaller than what is required to bridge the quantum jumps between successive steps. This is consistent with the nonlinear behavior observed in Figure 113.

Finally, the size dependence of the ascending velocity of intruders may find useful industrial applications, since it provides a means to separate particles immersed in a granular medium. We can envision the possibility of "filtering out" components of different sizes by a proper choice of the acceleration imparted to the cell.

5.3. Segregation by Shearing

As already mentioned, segregation by shearing, which comes about when two sheets of granular material slide past each other at different velocities, turns out to be surprisingly effective. The universal character of this phenomenon, involved in situations as diverse as geophysical processes such as landslides, mixing drums, and channeling through chutes, has prompted numerous recent investigations in two-dimensional configurations [98], [99]. Here again, we will restrict ourselves to the physics of the segregation of objects of different sizes, which is still in its infancy, as many seemingly simple phenomena remain unexplained. Segregation by shape, density, or micromechanical properties has not yet been studied thoroughly enough to warrant discussion in this chapter. We will begin with the behavior of a single intruder immersed in a uniform environment. This will be followed by an analysis of segregation in a mixture of two granulars of different sizes.

5.3.1. A Single Particle in a Uniform Medium

As pointed out in Chapter 4, a rotating drum is a convenient tool to study the flow properties of sheets of granular materials, and we will once again resort to this familiar device depicted in Figure 114 [98], [99].[10] This cylindrical drum with a horizontal axis is similar to the one that served us so well in Chapter 4 for studying avalanches. To take advantage of the image processing techniques described in Section 3.2.3, we want to select objects with a high visual contrast. For instance, we may use a matrix of white spheres and a single, black tracer particle, whose movements we wish to track. We learned in Chapter 4 that when the drum is rotated slowly about its axis, a series of more or less periodic avalanches of different sizes is set off. The avalanches are confined to a narrow layer near the free surface of the material, which constitutes what might be called a *liquid phase*. The rest of the structure is in a compacted state that can be thought of as a *solid phase*. The solid

[10]Figure 114 is a drawing, not a photograph taken during an actual experiment. The distinction is significant, inasmuch as it is not obvious that the configuration depicted here can truly occur in a real rotating drum. This particular structure was arranged so as to ensure the *local equilibrium* of every disk during the stacking process. There is a fundamental difference between that and the *global stability* of the entire edifice. An avalanche boils down to disrupting the local stability, which in turn affects the global stability of a granular pile.

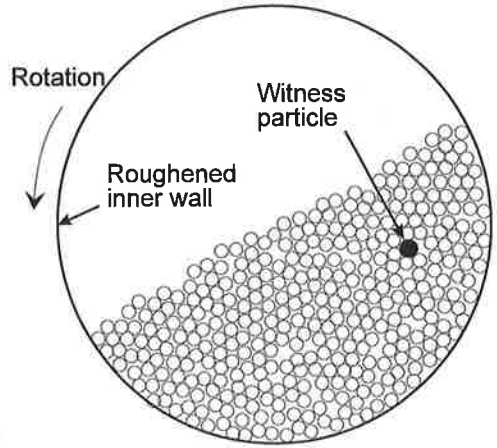

FIGURE 114. Typical experimental arrangement used to study segregation by shearing. We track the path of a tracer particle placed in a uniform matrix.

portion of the pile remains effectively bound to the cylinder. As the tracer particle is being dragged along by an avalanche to the bottom of the pile, it is reinserted and buried into the solid phase. The rotation of the drum then causes it to rise back up toward the free surface.

It is important to have a clear picture of the sequence of events. The evolution of the intruder is illustrated in Figure 115, which shows the outcome of a real experiment. The experiment reveals that the process of segregation toward the center or edges of the drum occurs in the flowing region at the surface of the pile. Based on what we know about avalanches, particularly about their statistical

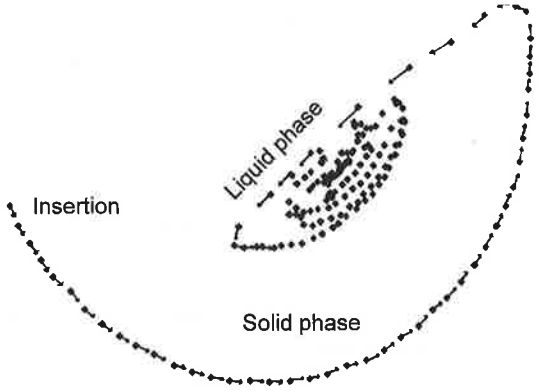

FIGURE 115. Velocity diagram of a tracer particle dragged in the liquid phase and reinserted in the solid phase. In the present case, $R < r$. The intruder is seen to converge toward the center (after [90]).

properties that we discussed in Chapter 4, we might expect that the reinsertion points should be randomly distributed at the surface. If so, a drum should be a very efficient mixer. As it turns out, this assumption is quite wrong, and we shall see shortly what experiments can tell us about why that is.[11]

From a practical standpoint, the question of segregation by shearing can be couched in the following terms: Given a tracer particle of radius R immersed in a bath of identical particles of radius r, what is the best experiment to do to find out what causes the tracer particle to either wander over the entire space available or, as the case may be, confine itself to a restricted portion of space, when the radii R and r are varied?

Once again, the answer to the question is provided by image processing techniques [99]. By tracking a marked intruder, it is possible to determine the rate of occupancy throughout the half-circle filled by the granular material in the drum. The measurement requires recording on the same image not only the various positions p_i of the marker, but also an indicator of how often each position p_i is occupied. This is done by assigning gray levels in such a way that the more often a site is visited, the darker the corresponding pixel appears. The technique involves the following series of steps:

(1) An image is recorded at time t_1. With suitable thresholding, the intruder is picked out and all other particles are discarded. This produces a map with a single black pixel.
(2) The brightness of the picture is then divided into 256, and the result is stored in a buffer (a block of memory in electronics parlance).
(3) A new image is recorded at a later time t_2. Its brightness is also divided into 256. This second image is added to the first one in the buffer. At this point, the buffer will contain either one pixel with a brightness of 2/256 if the intruder has not moved, or two separate pixels with a brightness of 1/256 if it has moved, in a sea of pixels with zero brightness corresponding to all the other sites that have yet to be visited.
(4) The cycle is then repeated from the top, for a total of up to 256 times.

The lower part of Figure 116 shows the results of this type of exercise. The data is analyzed by slicing time in discrete frames, denoted by an index i, during which one or more avalanches may occur. If the intruder is inserted in the flowing sheet at the radial coordinate r_i at time t_i, what will its coordinate r_{i+1} be in the very next frame at time t_{i+1}? The corresponding correlation diagram $r_{i+1} = f(r_i)$, referred to as the *map of first iteration*, is shown in the upper part of Figure 116. The diagram is drawn for a region encompassing a 40°-wide sector S, bounded on the short side by a radius R_1 corresponding to the exclusion zone of the particles in flow, and on the long side by the inner radius R_2 of the rotating cylinder.

[11] This is an important observation. It means that segregation by shearing does not result merely from reinsertion of an intruder during successive avalanches. A more plausible picture is for the intruder to undergo segregation by size during an avalanche and be transported across a distance that is determined by its relative size.

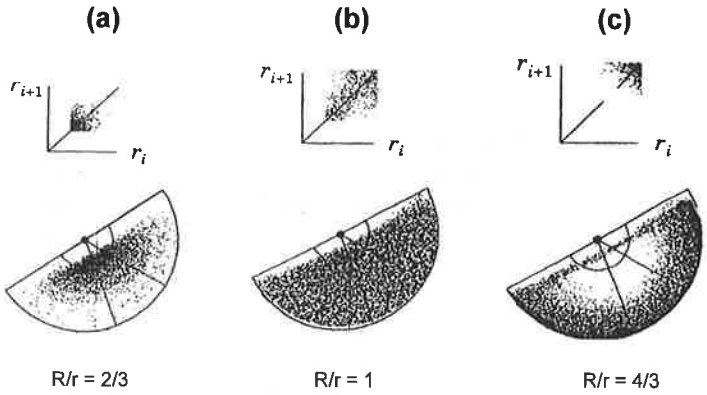

FIGURE 116. The bottom part of this figure is the superposition of 12,000 snapshots taken every 5 seconds. It shows the spatial distribution of the sites visited by particles whose diameter is (a) 1 mm, (b) 1.5 mm, and (c) 2 mm, placed in a bath of particles of diameter 1.5 mm. The upper part of the figure is discussed in the text. The cylinder had a diameter of 160 mm, and its rotation speed was typically 2 degrees/s (after [99]).

The results show that, depending on the size of the intruder relative to the majority particles, it tends to converge toward the center, to explore all the available space, or to take refuge near the periphery. A uniformly gray area indicates near perfect mixing.

We note first that the correlation diagrams $r_{i+1} = f(r_i)$ are all symmetrical with respect to the principal diagonal. This observation is not insignificant. It means that a true steady state is reached as early as the first iteration. If that were not the case, we would see over the course of measurements a flight of the intruder either toward large radii or toward small ones. That would translate into an accumulation of data points either above or below the principal diagonal in the correlation diagrams. It also means that the steady state can be described in terms of a relation of the type

$$\frac{\prod(r_{i+1}/r_i)}{\prod(r_i/r_{i+1})} = \frac{P(r_{i+1})}{P(r_i)},$$

where $P(r)$ is the probability of finding the intruder in region S, and $\prod(r_{i+1}/r_i)$ is the conditional probability of finding the particle at r_{i+1} when it is at r_i during the preceding frame. These results can be normalized by writing

$$P(r) = \int_{R_1}^{R_2} \prod(r/r')P(r')\,dr$$

and

$$\int_{R_1}^{R_2} P(r)\,dr = 1.$$

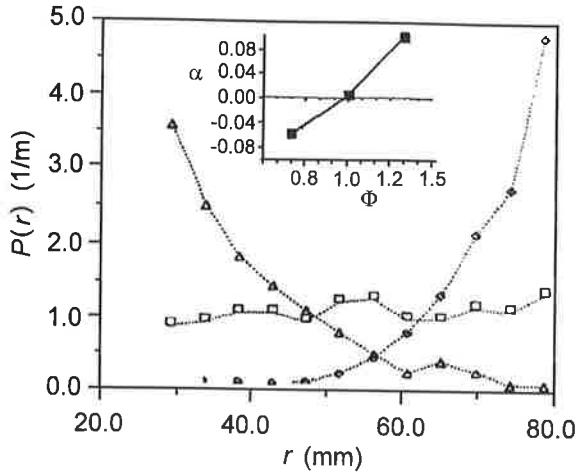

FIGURE 117. Probability of presence $P(r)$ in region S (see text). The triangles, squares, and parallelograms correspond to particles of diameter 1, 1.5, and 2 mm in diameter, respectively. They are immersed in a bath of particles whose diameter is 1.5 mm. The inset shows the dependence of the parameter α (the inverse of the localization length) on the diameter ratio Φ (after [99]).

The experimental results have been averaged over a distance Δr equal to three particle diameters.

Figure 116 shows convincingly that the region of space covered by the intruder depends on whether its diameter is larger or smaller than that of the majority particles. The same information is conveyed by a graph displaying the probability $P(r)$, as shown in Figure 117. To a first approximation, the probability $P(r)$ can be described by a function of the type $P(r) \propto \exp(\alpha r)$, where α represents the inverse of a length characteristic of the segregation process. Evidently, α changes sign when the ratio Φ goes through unity. A positive sign indicates that the intruder flees toward the periphery, a negative sign that it tends to converge toward the center.

Without pursuing the analysis of experimental results any further, we may note that our avalanche model discussed in Chapter 4 is not completely accurate. In particular, we had claimed that an avalanche, being of random size, should reinsert a particle anywhere along a flowing sheet. Actually, as revealed by the maps of first iteration or by tracking an individual marked particle of congruent size, both the center and the periphery of the cylinder are attractors for the dynamics of the system. If a particle is introduced near the periphery of the cylinder, it will tend to stay there. Likewise, a particle introduced near the center will tend not to wander off vary far. This implies a degree of correlation between trapping events taking place within avalanches, somewhat consistent with the model developed in Section 4.2.2. We might conclude that the dynamics of size segregation is governed by two attractors, one at the center, and the other on the periphery of the cylinder. According to this hypothesis, segregation in a rotating cylinder could be construed

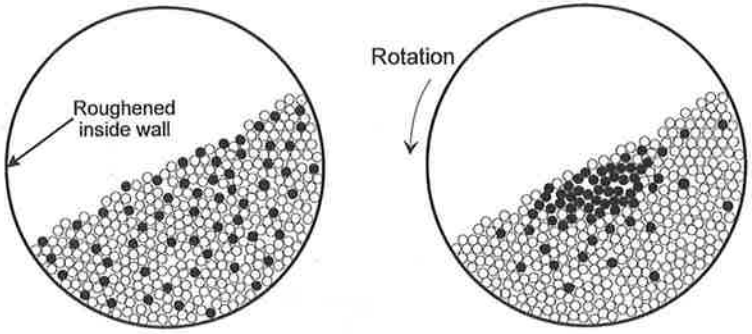

FIGURE 118. Schematic diagram of the segregation process of a two-dimensional granular mixture. The black particles are smaller than the white ones. They begin to collect near the center of the drum after just one revolution.

as a mechanism favoring one attractor over the other. Such situations often involve the phenomenon of bistability.[12]

5.3.2. *Segregation of Two Populations of Particles of Different Size*

We now consider a mixture of two distinct populations of particles. The first question that comes to mind is whether the observations just made in the case of a single intruder in a sea of identical particles can be extrapolated to predict the behavior of our mixture of two materials. In other words, can the process of separation in a binary mixture be treated as a succession of independent steps affecting individual particles, such as we were dealing with in the preceding section? The answer is not at all obvious, as we are about to find out. We will show that the kinetics and geometry of the segregation process depends on the shape of an incipient cluster growing with a fractal structure.

We now define the problem more rigorously. Let N_A be the number of particles of diameter d_A, which is to be mixed with, or segregated from, a number N_B of particles of diameter d_B. As usual, we define a ratio $\Phi = d_A/d_B$. The entire system is placed in a two-dimensional rotating cylinder of the type used earlier, which amounts to a simplified two-dimensional version of Oyama's drum. The experiment starts by mixing particles A as completely and randomly as possible with particles B. These may be, for instance, black disks mixed in with slightly larger white disks, as depicted in Figure 118.

The experiment reveals that after just a few turns of the cylinder, the smaller particles have gathered in the central part of the drum. The connected mass created this way is called the *reference mass*.[13] Its surface area, reached in principle

[12] A bistable system has two equilibrium states. It can switch from one to the other under the effect of some external perturbation.

[13] A mass is said to be "connected" when its particles actually touch each other.

after an infinite time—in reality, this time is quite short, as we will see—is denoted S_∞.

We proceed to highlight a few general ideas relevant to this situation. A more detailed analysis can be found in [90]. In order to characterize the state of the mixture, it is useful to introduce a parameter describing its degree of order. Let $S(t)$ be the surface area of type-A disks absorbed in the reference mass at time t. It is clear that $S(t)$ has to be smaller than S_∞. The degree of segregation is quantified by a parameter $a(t)$ defined as

$$a(t) \equiv \frac{S(t)}{S_\infty}.$$

At this point, it is natural to introduce an ordering parameter $P_o(t)$ that can vary between 0 (for a completely random and homogenous mixture) and 1 (for a fully developed reference mass). This parameter is defined in terms of $a(t)$ by

$$P_o(t) = \frac{a(t) - a(0)}{1 - a(0)}.$$

$P_o(t)$ can easily be determined by means of imaging processing techniques of the type described in Section 3.2.3. The results presented in Figure 119 shed some light on the kinetics of the process of segregation.

The graph reveals two important findings:

- The growth of the ordering parameter is surprisingly fast. With a rotation velocity as low as 1.3 rpm, the reference mass is virtually fully developed after only about 100 s, which corresponds roughly to two full turns. The time constant τ in Figure 119 is of the order of 0.7 revolution. These results underscore the remarkable efficiency of segregation by shearing.

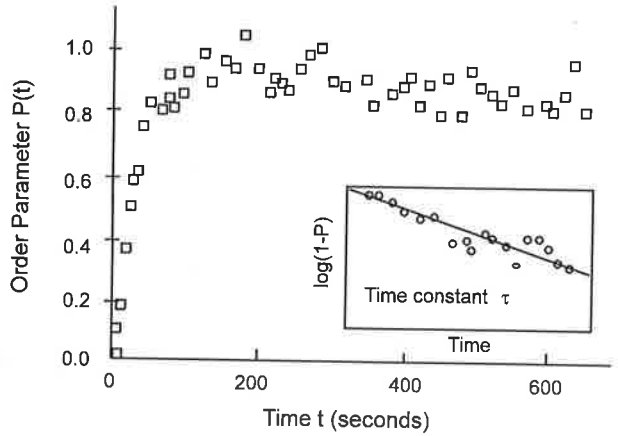

FIGURE 119. Order parameter $P_o(t)$ plotted against time for a mixture of disks with diameters of 6 and 10 mm. Thirty percent of the surface is occupied by the smaller disks. The inset shows the dependence of $[1 - P_o(t)]$ on time (after ref. [90]).

- The ordering parameter grows exponentially. The inset in Figure 119 shows that it evolves as $P_o(t) \propto 1 - \exp(-t/\tau)$, which describes a kinetic process of first order. This remarkably simple behavior remains totally unexplained.

When studying mixtures of different concentrations of particles A and B, the conclusion is that the time constant τ is practically independent of the composition. As of yet, this too is unexplained.

Segregation Speed and Particle Size

The ratio of the diameters of the two types of particles should play an important role in how fast the central mass forms. Indeed, we know the result in two extreme cases:

- When the ratio Φ is quite small (typically less than 0.2), which happens when one type of particle is very much smaller than the other, a phenomenon known as *sifting* takes place. It describes the ability of the smaller particles to snake their way through the interstices between the larger ones. This situation can be modeled using the concepts of *directed percolation*. The small particles then remain trapped at the interface between the liquid and solid phases which defines the flowing sheet. Since the medium in which the small particles evolve is defined by the gaps between the large ones and is, therefore, independent of their own size, the ratio Φ should have no effect on the velocity of segregation. Under these circumstances, the time constant τ must be independent of Φ.
- If the ratio Φ is such that $\Phi = 1$, which amounts to dealing with a single type of particle, the arguments developed in Section 5.3.1 apply. In particular, we established that all particles roam through the entire space available. By marking some of the particles, it was subsequently established that particles actually tend to remain in the vicinity of the attractor nearest the point of insertion. If so, it is, of course, impossible to cling to the definition of the parameter τ. It must diverge to infinity since, from a macroscopic point of view, P_o is required to remain constant in this case.

Numerous experiments have shown that between these two extremes, the time constant τ varies approximately linearly with the ratio Φ. If τ is expressed in numbers of rotations, then we have the simple linear relation

$$\tau \approx 1.2\Phi \qquad \text{with} \quad \Phi \in [0.2, 0.8].$$

This expression does indeed give $\tau \approx 0.7$ when $\Phi = 0.6$.

We conclude this section, devoted to segregation by shearing, with a discussion of the surprising—and so far unexplained—dependence of the time constant on the rotation velocity of the drum which, up to this point, has been held constant at 1.3 rpm.

Segregation Speed and Rotation Velocity

First off, we note that a rotation speed of 1.3 rpm, chosen for the experiments described above, causes a continuous flow along the tilted surface in the drum.

This is entirely consistent with the results reported in Section 4.1, namely, that the flow switches from discontinuous to continuous at around 0.3 rpm. Second, the speed of 1.3 rpm is well below the 12 rpm needed for the onset of inertial effects.

Both the previous experiments and the present one were done with 600 small disks 6 mm in diameter, and 720 large disks 10 mm in diameter, giving area ratios of 25% and 75%, respectively. Two surprising results emerged. First, the time constant remained unchanged at 25 s as the rotation velocity varied from 1.3 to 8 rpm. Second, at velocities higher than 8 rpm, segregation disappeared altogether and the mixture remained substantially homogeneous, even over periods of several hours.

These results are completely unexpected and, for the time being, without explanation. We would normally anticipate that the process of segregation should become more efficient as the small disks pass more frequently through the portion of granular material flowing down the slope. In fact, nothing of the sort happens. Quite on the contrary, segregation proceeds at the same pace even though the number of crossings through the liquid phase varies by more than a factor of 6. Furthermore, since segregation was shown to behave as a kinetic process of first order, we would expect it to depend monotonically on rotation speed, rather than to suddenly drop to zero at 8 rpm.

Perhaps a plausible interpretation can be proposed if we go back to the principles we invoked to explain the role of arch effects in the phenomenon of segregation by vibration. We argued that a granular system must have enough time to relax between excitations in order to adapt to the intruder's geometry. Only then can the intruder migrate efficiently. In other words, segregation is sensitive to the size and geometry of the objects involved and requires a finite amount of time to manifest itself. When viewed in that light, the results described above may not be so puzzling after all. As the rotation velocity increases, the granular surface flow becomes too fast and chaotic, leaving too little time to adjust to the geometry of the particles. We may even push the argument a step further and envision that the flowing sheet, which is liquid-like at low speed, gradually turns into a gas as the number of collisions between particles increases with speed. This hypothetical "phase change" between liquid and gas may occur rather abruptly and could very well explain why segregation suddenly disappears above a certain rotation velocity (in the present case, at 8 rpm). Between 1.3 and 8 rpm—the regime where segregation proceeds efficiently—the experimental results show that τ increases linearly with rotation velocity (provided that τ be expressed in number of revolutions).

Fractal Growth of the Central Cluster

As we noted earlier, the central cluster made of the smaller particles is practically formed in a very short time corresponding to two revolutions of the cylinder, or just three times the time constant τ. Having determined that, for all practical purposes, the formation of this cluster is governed by a first-order law, as are many other growth processes, we set out to try to understand the phenomenon on the basis of geometrical considerations.

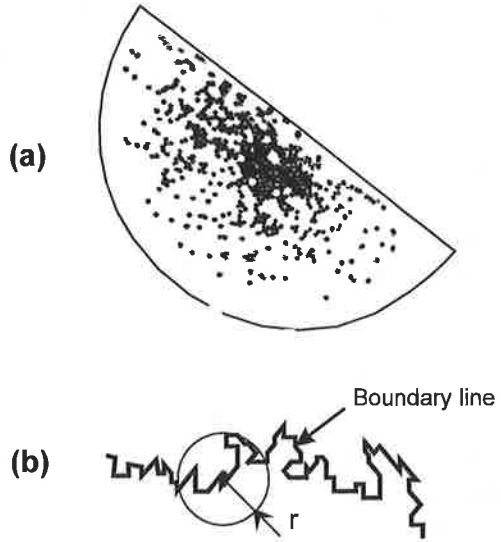

FIGURE 120. Diagram (a) shows particle clustering after the drum, filled as indicated in the text, has rotated for 300 s. Diagram (b) shows a portion of the boundary of the accumulated cluster.

There exists a prolific literature on the subject of materials synthesis by a variety of growth mechanisms, including thin-layer deposition, Diffusion-Limited-Aggregation (or DLA, for short), [100]-directed percolation, and several others. Quite often, these various growth mechanisms lead to self-similar geometrical forms, that is to say, structures with fractal properties.

Defining the segregated cluster as that delineated by the greatest possible number of connected points, we designate by $M(r)$ the length of the jagged line that forms its boundary. The objective is to calculate this length as a function of the radius r of a circle centered on a particular point of the line, as shown in Figure 120. Let $M(r_s)$ be the length obtained when the radius r of the circle matches the radius r_s of the small disks composing the segregated mass. We can then generate diagrams of the quantity $\log[M(r)/M(r_s)]$ plotted against $\log(r/r_s)$. The result is shown in Figure 121. The graph reveals that the boundary of the segregated cluster has a fractal structure with a dimension $d = 1.62 \pm 0.2$, which allows us to write the functional dependence $M(r) \propto r^d$.

As it happens, numerical simulations have also been done, although in a somewhat different context [100]. Based on a model of directed and uncorrelated growth of a two-dimensional structure, they gave an exponent of 1.76, not too different from the result reported above. It can be shown, incidentally, that the exponent should decrease when finite-size effects are present, which is most certainly the case for our segregated cluster. To be sure, these considerations are only semi-quantitative. Although they have great pedagogical value, the results described here have yet to be confirmed by more careful experimental work and further theoretical analysis.[14]

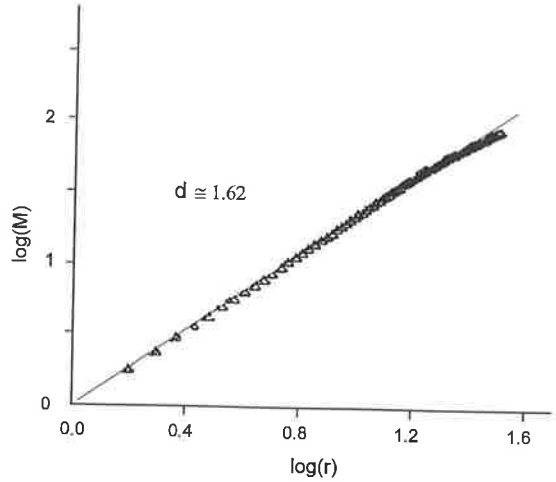

FIGURE 121. Normalized length M plotted against the radius r of the measurement circle.

5.4. Segregation in Oyama's Three-Dimensional Drum

As noted at the beginning of this chapter, the experiment reported in 1939 by Oyama involves a phenomenon that remains without explanation [89]. A schematic diagram of the experiment is reproduced for convenience in Figure 122. The reader will recall that an initially homogeneous mixture of two kinds of particles with different sizes gets segregated in vertically separate regions as the drum rotates. The physics of this phenomenon has so far defied analysis.

We will first describe a few experimental observations reported in the literature [90], [101]. We will then sketch the broad outlines of a model recently proposed by S. Savage [102].

5.4.1. *Experimental Observations*

The experiments described here are done by filling one-third of the volume of a glass cylinder 70 cm long and 10 cm in diameter, whose internal wall is lined with roughened spheres. The mixture introduced into the cylinder is composed of 50% of colored spheres 1 mm in diameter, and 50% of spheres of a different color and 3 mm in diameter. The cylinder is then rotated around its horizontal

[14] De Gennes has recently developed a model for segregation via avalanches [43]. The model is based on a set of coupled variables discussed in Section 4.2.3. Although it deals with a situation that is different from a rotating drum, it leads to power laws with fractional exponents which may well have a bearing on the experiments described here.

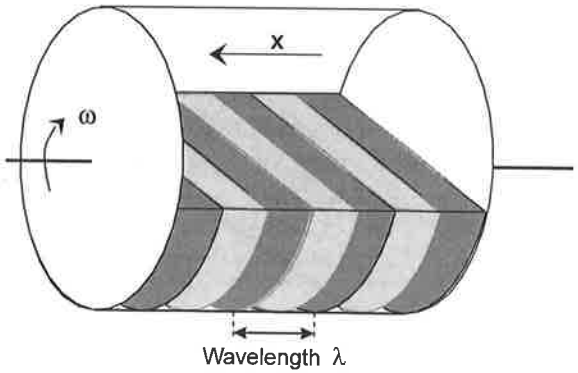

FIGURE 122. Three-dimensional segregation in Oyama's drum. An initially homogenous mixture of two different types of particles undergoes segregation in a number of bands perpendicular to the axis of rotation.

axis at speeds ranging from 15 to 65 rpm. After 10 or 20 min, the mixture has separated in bands characterized by a wavelength λ, as depicted in Figure 122. The most salient features of the experimental results can be summarized thus: Between 15 and 65 rpm, there is little or no dependence of the wavelength on the angular velocity. When the rotation speed drops below 15 rpm, segregation ceases altogether, and the smallest bands tend to be the first ones to vanish.

Several authors have reported that the steady state, reached after long periods, consists of three bands.

5.4.2. *Savage's Model*

S. Savage has proposed a phenomenological model based on an observation we skimmed over briefly in Section 4.1. It refers to a phenomenon that is observed fairly frequently but is poorly understood [103], [104]. Specifically, when the drum is rotated at a speed sufficient to generate a continuous flow, the tilt angle of the surface sheet with respect to the horizontal depends on the size of the particles. Whether this reflects a kinetic drag phenomenon or, as is more likely, a finite-size effect typical in this type of experiment, the fact the kinetic angle changes according to the type of particles will induce a lateral flux (i.e., parallel to the x-axis in Figure 122), which will depend on the ratio of the particle diameters as well as on the rotation speed.[15] With this observation in mind, we consider a mixture of two populations of spheres A and B. Let θ_A and θ_B be their respective kinetic angle at a given rotation speed. We denote by $C_A(x)$ the local concentration of species A at a point of abscissa x. We expect the kinetic angle $\theta(x)$ of a mixture of particles to be a weighted average of the kinetic angles of each individual species.

[15]Curiously, the dependence of the kinetic angle on particle size has apparently never been observed in two-dimensional geometries, perhaps because the total number of particles is then too limited. Expanding on an idea advanced in Section 4.1 in connection with avalanches of various sizes, we may surmise that the aspect ratio manifests itself only when the number of particles is large enough, regardless of dimensionality.

This we write

$$\theta(x) = \theta_B + \Delta\theta C_A(x)$$

with

$$\Delta\theta = \theta_A - \theta_B.$$

Focusing our attention on type-B particles, their flux will result from two competing effects. On the one hand, there is a flux $\Phi_{Bx}(\Delta\theta)$ due to the difference in kinetic angles, which tends to drive particles along the direction of the x-axis (see Figure 122). On the other, there is an opposing flux Φ_{BD} due to diffusion and described by Fick's law involving a diffusion coefficient D. The total flux Φ_{Bx} of B-type particles along the x-axis is then given by

$$\Phi_{Bx} = -\Delta\theta \frac{\partial C_B}{\partial x} - D\frac{\partial C_B}{\partial x}.$$

To summarize, the horizontal flux is created by differences in the kinetic angle, but it is opposed by a diffusive component that tends to equalize the concentrations. The formation of bands would result from competition between the two effects.

6

Numerical Simulations

6.1. Introduction

Numerical simulations aimed at modeling various aspects of the physics of granular materials, which we have touched upon throughout the earlier chapters, have a twofold objective.[1] On the one hand, there are pressing incentives to solve a number of practical problems related to the treatment of granular matter in industry. Whether the issue is pesky segregation, blockages of flows by arch effects, or disruptive internal convection phenomena (see Chapter 1), the requirements of the industrial sector are many and, needless to say, almost always immediate. The urgency of industry's needs and the increasingly rapid developments of creative numerical simulation techniques have prompted many researchers to devote a great deal of effort to devising algorithms suitable for describing the behavior of granular materials.[2]

On the other hand, numerical simulations are of considerable interest from a more fundamental point view as well. They offer the possibility to explore the effect of many parameters which are simply not accessible to experimentation.[3] In that sense, numerical simulation has truly become an integral part of basic

[1] An excellent introduction to the topic of numerical simulations of granular materials can be found in [59].

[2] At the present time, the number of researchers engaged in numerical simulations in this particular domain of physics substantially exceeds those pursuing experimental work.

[3] That is the case, notably, for the coefficients of elastic restitution ε and the coefficients of friction μ, which can be varied at will on a computer, whereas nature offers the experimenter a very limited range of choices.

research. Indeed, it does not operate in a vacuum. Comparing experimental results and numerical simulations constitutes the ultimate test to validate—or reject, as the case may be—tentative models.

The goal of computer modeling is as ambitious as it is clear. Starting from the properties of the elementary granules that make up the material of interest, and incorporating whatever may be known about their mutual interactions, the objective is to devise computational methods flexible and general enough to predict the actual behavior of a real granular system in a variety of situations.

6.1.1. *The Challenges of Numerical Simulation*

The comments we have just made could apply just as well to any other area of the physical sciences. Yet, the case of granular materials is rather unique. We have already hinted in Chapter 2 at the difficulties physicists face when trying to model collisions and friction between solids. Modern numerical techniques can deal with so-called n-body problems, even when n is quite large. That is no longer an obstacle. The main challenge is to incorporate in the formulation of these problems the basic micromechanical properties describing the relevant interactions, and to do so as accurately as possible. Many decisions have to be made while setting up a model. What is the duration t_c of a collision between two particles? What is the penetration distance (Section 2.2.2)? How should the proper time step be chosen in relation to both the time interval between two successive events and the collision duration t_c (Sections 2.2.2 and 3.2.1)? What is the best way to model Coulomb's laws of dry friction (see Section 6.4)? Perhaps the toughest problem of all is how to account correctly for the effect of microcontacts and their erosion over time, as mentioned in Section 2.2.1. Is there a way to include phenomena of wear and tear and strain hardening in the model? All these questions have to be answered before devising a realistic simulation.

6.1.2. *The Different Simulation Methods*

Given this lengthy list of problems inherent to granular materials, it is hardly surprising that a great many different strategies have been proposed over the last few years. As it turns out, each simulation method has its advantages and drawbacks. Whether it be in terms of computational time or accuracy of results, no approach developed to date can satisfy all requirements. Compromise is the rule, as each method suffers from some degree of limitation. Under these circumstances, choosing one over another requires a good deal of caution.

Coming up with a logical classification scheme of such diverse simulation techniques is no easy task. It would be a bit presumptuous to attempt a comprehensive review of everything we presently know on the issue of simulating granular matter. Without exceeding the scope of this book, though, it is possible to extract from simple observations a few general principles which we will build on in the remainder of this chapter. This approach will enable us to clarify a number of notions which those doing simulation work routinely rely on.

Hard Spheres and Soft Spheres

The first idea that comes to mind to simplify the level of difficulty in modeling solids in collision is to treat them as hard spheres. In the context of numerical simulation, however, the word "hard" does not necessarily imply that the collisions are perfectly elastic. It simply means that there is no interpenetration or deformation during impact, which is considered infinitely brief. The loss of linear momentum is characterized solely by means of the coefficient of elastic restitution, at least when rotations are neglected. That was in fact the approach we used to model a column of spheres in Section 3.2.1.

The *hard-sphere* approximation is at the basis of the so-called "collisional" or "event-driven" (ED) models, as we will see later on. It is also the principle behind various pile-synthezing methods, including *dynamics of contacts* (see Section 6.4), *Monte Carlo*, and *steepest descent*.

In this approach, the mechanisms of restitution of elastic energy and friction are treated as if they were completely decoupled. Dry friction is generally modeled in terms of Coulomb's laws as presented in Section 2.2.1.

The *soft-sphere* approximation is based on an entirely different principle. Here, friction and elastic restitution come into play only when spheres penetrate into each other, and the magnitude of the interaction depends on the penetration depth. The prototypical algorithm in this category is the *molecular dynamics* (MD) model. The essence of this approach revolves around the deformation of spheres. As such, how long they remain in contact is of paramount importance.

Duration of Collisions and Chronology Problems

Predictably, the order in which the calculations are performed must be selected with care. Two possibilities exist, each with its own advantages and disadvantages:

- The first option consists in sampling the system at regular intervals, using a time step small enough to avoid "missing" an event, which could completely change the subsequent chain of events. However, as we have already pointed out, the duration of contact between hard spheres is infinitesimally short. Several collisions may occur in rapid succession and possibly set up oscillations at a rate exceeding the sampling frequency, as suggested in Section 3.2.1 and illustrated in Figure 123. Therefore, a sequential algorithm is not a wise choice in the hard-sphere approximation. It would be more suitable for a *molecular dynamics* model, where collisions have a finite duration.
- Researchers have devised an algorithm in which the timing of the sampling is governed not by a fixed external clock, but by events themselves. This type of event-driven approach guarantees that no event will be missed. On the downside, there is a risk of getting trapped in situations where a particular event, such as an oscillation triggered by a collision, lasts for a very long time. It then becomes necessary to rely on some test criterion to get around the trap. We have already mentioned such a criterion in Section 3.2.1, known as LRV (Largest Relative Velocity).

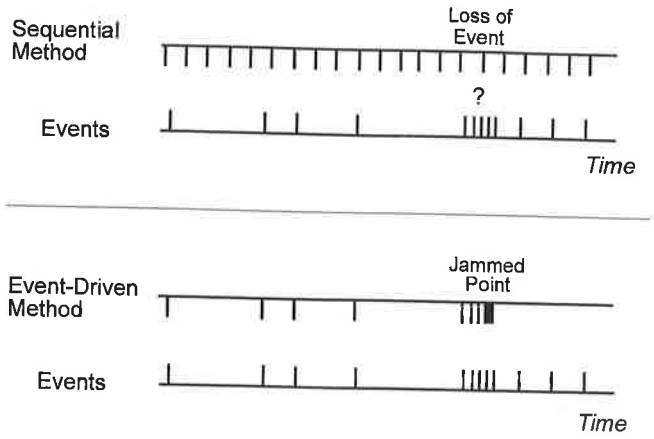

FIGURE 123. Schematic illustration of the type of difficulties encountered in numerical simulations using either sequential algorithms (top) or event-driven algorithms (bottom).

Summarizing, ED-type algorithms are particularly well suited to describe hard spheres, while MD algorithms, based as they are on soft spheres, are more compatible with regularly spaced periodic sampling. The remainder of this chapter will provide more details on these two techniques, which have become widely used. Next, we will describe briefly some approaches based on the mechanical properties of contacts between solids, coupled with specific convergence criteria. This latter approach has recently scored some remarkable successes in modeling the dynamics of granular structures in a variety of situations. In connection with the Brazil nut problem, we will describe the *Monte Carlo* technique, as well as the method known as *steepest descent*. Finally, cellular automaton models have also been proposed recently to simulate the dynamics of granular materials. They are close cousins of those used so successfully in solving certain hydrodynamics problems. This area is currently in rapid development, and it would be premature to cover it in great depth.

Before embarking on an analysis of these various techniques, this is an appropriate opportunity to provide at least a partial answer to a question we have raised on several occasions in the preceding chapters: How to make the transition from a discrete representation—which a numerical simulation is by essence—to a "thermodynamical" description of a granular medium?

6.1.3. The Transition from a Discrete to a Continuous Description

We have emphasized in Chapter 3 the difficulties faced by continuum descriptions when applied to a real granular medium, which is inherently discontinuous. Predictably, differential equations become increasingly inadequate as the number of particles involved diminishes. This type of problem was particularly evident in our analysis of granular avalanches in Chapter 4.

Numerical simulations modeling a sequence of events such as collisions and friction determine at any given instant the position x_i and velocity u_i of every particle. On the other hand, we know that classical thermodynamic theory rests on continuous and differentiable variables such as density ρ, collective drift velocity v, and macroscopic temperature T. The question is whether there exists a connection between the two types of description. Given a complete knowledge of the positions and velocities of all the particles (provided by a numerical simulation), is there a way to define the thermodynamic quantities ρ, v, and T?[4] Symbolically, we may write

$$\begin{Bmatrix} x_i \\ u_i \end{Bmatrix} \overset{?}{\Leftrightarrow} \begin{Bmatrix} \rho \\ v \\ T \end{Bmatrix}.$$

There are clearly several possible answers to this question, some more realistic than others. The technique we describe next has the merit of being fairly intuitive. It is rooted in the notion of "cloud," which effectively spreads out the mass of each particle over a region larger than its actual volume [57]. In this picture, the clouds associated with two particles can overlap, which ensures a continuous passage from one to the other. The cloud function $h(r)$ must satisfy several conditions. They are

$$\int_0^\infty h(r) 2\pi r \, dr = 1, \tag{6-1}$$

$$h(r) \to 0 \quad \text{when} \quad r \to \infty, \tag{6-2}$$

$$h(r) \geq 0. \tag{6-3}$$

Equation (6-1) is the normalization condition, written here in two dimensions, (6-2) states that a cloud is primarily localized around its associated particle, and the inequality (6-3) ensures that the density ρ and temperature T will be positive quantities. To simplify the calculations, we adopt a Gaussian distribution for the cloud function $h(r)$

$$h(r) = \frac{1}{2\pi\sigma^2} \exp\left(-\frac{r^2}{2\sigma^2}\right),$$

where σ is larger than the diameter d of a particle (for instance, $\sigma = 6d$) and determines the extent of the clould. This enables us to define a density ρ, a macroscopic

[4] We have already defined in Section 4.2.1 a granular temperature as the driving force of a thermal agitation by vibration which causes the detrapping necessary to set off an avalanche. It is not in the least proven that this definition is identical to the one we are about to put forth in this section.

velocity v, and a temperature T, through a series of three successive equations

$$\rho(x) = m \sum_{i=1}^{N} h(|x_i - x|),$$

$$\rho(x)v(x) = m \sum_{i=1}^{N} u_i h(|x_i - x|),$$

$$\rho(x)T(x) = m \sum_{i=1}^{N} \frac{u_i^2}{2} h(|x_i - x|) - \rho(x)\frac{v^2(x)}{2},$$

where N is the number of particles used in the simulation, and m is the mass of each. These macroscopic quantities are continuous in space and time. It is possible to calculate their gradients, and as such they can be viewed as the usual thermodynamic variables.

6.2. Simulations of Collisions

6.2.1. *Introduction*

As we saw in Chapter 3, event-driven (ED) methods consist in establishing a set of general equations describing the dynamics of the system (for instance, Newton's equation, as spelled out in Section 2.2.2). Knowing the variables $\{x_i, v_i\}$ for all particles during a particular event, the next chronological event can be predicted, and the procedure is repeated sequentially. Section 3.2.1 described the use of this technique to model a one-dimensional pile of hard spheres in vibration. We subsequently saw the same technique applied to problems of decompaction and self-organization (Section 3.2.4). We will not dwell on this method any further. The interested reader is encouraged to go back to the cited sections to review the details. What we will do here is describe a procedure to get around problems of accumulation which were mentioned before.

6.2.2. *One-Dimensional LRV Procedure*

The so-called LRV procedure (for *Largest Relative Velocity*) is useful when granules in a multiparticulate system come in contact and form what we have referred to as *blocks* [59]. The power of the technique lies in its ability to avoid infinite computational loops that arise when the particles, assumed to be made of hard spheres, remain clustered. The algorithm relies on a logical test to make predictions about the outcome. As such, it avoids situations that would result in impractically lengthy calculations.[5] Figure 124 illustrates a specific case.

[5] Researchers doing numerical simulations frequently resort to such predictive techniques, which consist in bypassing accumulation points leading to endless loops by deciding ahead of time the state a system will find itself in. This type of trick, as it were, speeds up the computation time. It only works, of course, to the extent that the predictions are indeed correct.

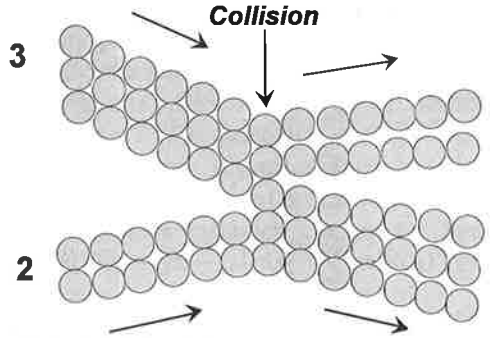

FIGURE 124. Evolution of a group of five spheres, initially grouped in two blocks, for $\varepsilon = 0.8$ (after [59]).

Consider five spheres originally arranged in two blocks of two and three members, respectively, about to collide. What is the trajectory of the five spheres after the collision? Do the spheres coalesce into a single block? If not, do they separate and perhaps rearrange themselves in a different pattern? Before solving this problem, it is useful to recall the definition given earlier of a "block" in the context of a numerical simulation. Two colliding particles form a block if their relative velocity is smaller than a predetermined value v_c chosen according to the characteristics of the computer used. From a practical standpoint, the velocity differences between all pairs of adjacent particles forming a block have to be computed at every instant identified by the ED algorithm. Let $\Delta v_i = v_{i-1} - v_i$ designate those differences for all adjacent pairs of a block. Pairs for which $\Delta v_i < 0$ do not collide, while those for which $\Delta v_i > 0$ are likely to. The LRV procedure works as follows:

(1) We pick the adjacent pair with the largest value of Δv_i, or $\Delta v_j = \max(\Delta v_i)$, at the moment of impact, and we let the particles $(j, j-1)$ collide.
(2) Collision matrices of the type described in Section 3.2.1 are used to calculate an updated set of differences Δv_i.
(3) The previous two steps are repeated until all the differences Δv_i become either smaller than v_c (in which case the corresponding particles form a block) or negative (in which case they fly apart).

It has been shown that this type of predictive approach does indeed lead to the same result as the conventional ED method.

6.3. Molecular Dynamics (MD) Simulations

The so-called molecular dynamics (MD) methods benefit from a large menu of algorithms developed and tried in many different test cases. It is fair to say that this technique has matured to the level of an indispensable tool to simulate many aspects of the dynamics of granular materials, provided that certain precautions concerning time and spatial scales be taken. The technique relies on the concept

of soft spheres and on a sequential calculation. The primary difference with event-driven methods is that in the present case the duration t_c of a collision is not zero. The principle behind MD methods is to solve in regular incremental steps the equations governing the changes in linear and angular momenta of the colliding particles. The objective is to solve the following vector equations

$$\Delta p = \Delta(mv) = mv - mv_0 = \int_0^{t_c} F_{\text{cm}}\, dt \tag{6-4a}$$

and

$$\Delta(I\omega) = I\omega - I\omega_0 \int_0^{t_c} (r \times F)\, dt, \tag{6-4b}$$

where I is the moment of inertia of the solid around its axis of rotation, $r \times F$ is the torque exerted by the force F, and F_{cm} is the component of the force acting on the center of mass. Once again, we emphasize that this strategy is quite different from the one followed in ED models, which starts from the equations governing momentum exchanges, in the manner described by (2-2) and (2-3). In the present case, solving (6-4) requires a knowledge of the forces F and F_{cm}, of how they vary in time, and of the duration t_c of the collision. As a prerequisite to any molecular dynamics simulation, it is essential to model as exactly as possible the forces of elastic restitution and friction involved during collisions between particles. We have already stressed on numerous occasions how fundamentally difficult this task can be (see, in particular, Section 3.1.1), due to the inherently indeterminate nature of the equilibrium forces in a granular stack, as they depend on its prior history, or to our limited understanding of contact interactions between solids. This explains the many forms of equations proposed by various researchers working on this problem. The situation is not unlike that discussed in Section 4.2.2, in which we reviewed a variety of functional dependences of the friction forces on velocity.

The goal of the next few paragraphs is to discuss the different types of behavior we might encounter in modeling the contact forces F and F_{cm}, which feed directly into (6-4).

6.3.1. *Elastic and Friction Forces*

Linear and Nonlinear Equations

Consider a set of N spherical particles of diameter d_i, where the index i runs from 1 to N [59]. If the particles are all identical, we obviously have $d_i = d$ for all values of i. We can also envision without any difficulty a distribution (for instance, Gaussian) of diameters d_i centered on a value d and with a spread $\langle \Delta d \rangle$. Let r_{ij} be the distance between the centers of two particles of index i and j. In accordance with Signorini's conditions, which are widely used in matters pertaining to the mechanical properties of contacts (see Section 6.4), the forces of contact come into play only when $d_i + d_j < 2r_{ij}$. When this condition is verified, three different

contact forces are involved, at least under the assumption that angular momenta can be neglected. In simplified vector notation, these forces are:

- A *force of elastic restitution*, related to the elastic energy stored during the penetration of the two particles. This force is given by

$$\mathbf{f}_{el}^{(i)} = -K\left[\tfrac{1}{2}(d_i + d_j) - r_{ij}\right]\mathbf{n}_{ij}, \tag{6-5}$$

  where $\mathbf{n}_{ij}$ is the unit vector along the line connecting the centers of the particles i and j. This is simply the usual relation for the deformation of a spring with stiffness K. It is obviously linear and, as such, incompatible with Hertz's penetration model (Section 2.2.2), which predicts a power law with an exponent of $\frac{3}{2}$ to describe how the force depends on the penetration distance. To allow for this nonlinearity, (6-5) is modified to a slightly more general form

$$\mathbf{f}_{el}^{(i)} = -K\left[\tfrac{1}{2}(d_i + d_j) - r_{ij}\right]^{1+\beta}\mathbf{n}_{ij}, \tag{6-6}$$

  where $\beta = \frac{1}{2}$ in the Hertz model, and $\beta = -\frac{1}{2}$ in the case of a soft crust (see Section 2.2.2).
- A *friction force* which opposes the rupture of contacts. It plays a dissipative role similar to that of the Euler–Coulomb dynamic friction. For generality, two components are distinguished. The normal component is

$$\mathbf{f}_{n}^{(i)} = -2D_n m_{ij}(\mathbf{v}_{ij}\cdot\mathbf{n}_{ij})\mathbf{n}_{ij}, \tag{6-7}$$

  where m_{ij} is the reduced mass of the system of two colliding particles i and j, $\mathbf{v}_{ij}$ is the difference between their velocities, and D_n is a dissipation coefficient characterizing the separation of contact along the direction of $\mathbf{n}_{ij}$. Likewise, the tangential component of the friction force is

$$\mathbf{f}_{t}^{(i)} = -2D_t m_{ij}(\mathbf{v}_{ij}\cdot\mathbf{t}_{ij})\mathbf{t}_{ij}, \tag{6-8}$$

  where $\mathbf{t}_{ij}$ is a vector tangent to the contact, that is to say, perpendicular to $\mathbf{n}_{ij}$, along the slip direction, and D_t describes the corresponding dissipation.

Here again the linear approximation contained in (6-7) and (6-8) is sometimes too limiting. The equations are often generalized in the form

$$\mathbf{f}_{n}^{(i)} = -2D_n m_{ij}(\mathbf{v}_{ij}\cdot\mathbf{n}_{ij})\left[\tfrac{1}{2}(d_i + d_j) - r_{ij}\right]^{\gamma}\mathbf{n}_{ij},$$

valid only when $\frac{1}{2}(d_i + d_j) > r_{ij}$.

It is extremely important to understand that dissipative processes introduced in these equations to model friction are inherently *dynamic* in nature. Indeed, these equations do not account for Coulomb's static friction forces. The present model applies exclusively to a dynamic analysis of granular piles, as does the ED technique discussed earlier.

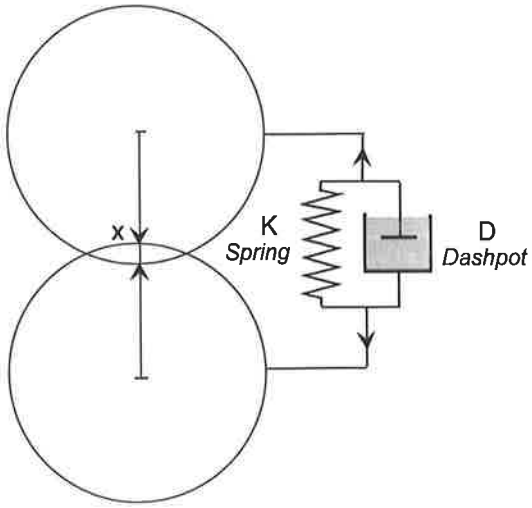

FIGURE 125. Mechanical model simulating contact interactions by a coupled spring–dashpot arrangement. The dashpot acts as a shock absorber.

Mechanical Analogies

The preceding equations were introduced purely phenomenologically. They may, however, be interpreted in terms of more concrete models that give a physical meaning to the parameters figuring in the equations. The simplest analogy is depicted in Figure 125. It features a spring (simulating elastic restitution) coupled to a linear dampener.[6]

Such a simple system obviously cannot account for the subtleties of contact interactions, such as the plastic deformations that typically occur when two colliding spheres penetrate each other, as pointed out in Section 2.2.2. More elaborate variants have been proposed to simulate these more complicated effects [38]. An example is depicted in Figure 126. With enough creative imagination, other arrangements can undoubtedly be contrived, but we should keep in mind that such mechanical analogies have limitations and remain crude pictures of reality. Figure 126(b) describes the behavior of the system shown in Figure 126(a). The spring of stiffness K_1 is compressed, simulating the two particles colliding and penetrating each other. On Figure 126(b), the operating point moves up along the straight line of slope K_1 until its abscissa is equal to α. At that point, the ratchet mechanism jumps down one notch, which causes the stiffness to suddenly increase to K_2. If the system is allowed to relax in its new configuration, the operating point moves back down along a different line of slope K_2, until it reaches the point of abscissa α_0. Since the force has now returned to zero, the system is clearly left in a different state relative to what it was, which is consistent with the phenomenon of

[6] Such a dampener is sometimes referred to as LSD, for *linear spring dashpot*. Those fond of acronyms will shortly be treated to an example of PLS, for *partially latching spring*.

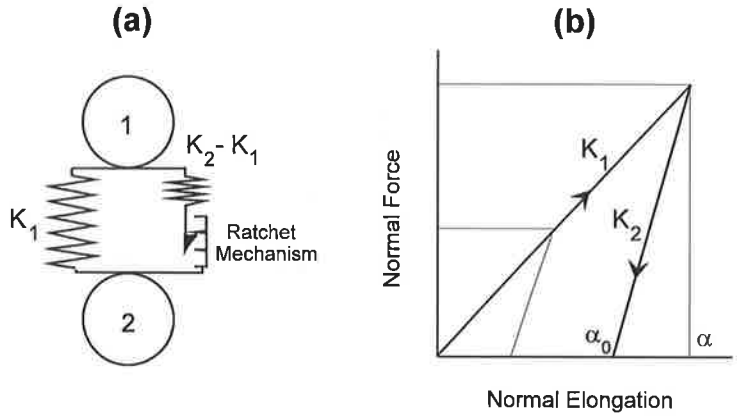

FIGURE 126. Mechanical model of the phenomenon of plasticity. It uses a set of coupled springs, one of which activates a ratchet mechanism.

plastic deformation. As more and more notches get engaged, the operating point describes increasingly skinny triangular sectors, as shown in Figure 126(b). The plastic limit corresponds to the first notch on the ratchet. As long as that condition is not exceeded, the regime remains linear with a stiffness K_1. Beyond that point, two offset springs act in parallel, with a net stiffness $K_1 - K_2$. As intriguing as this device may be, it still cannot reproduce Hertz's nonlinear penetration regime.

6.3.2. *MD Collision Model*

This section deals with the equations that govern the collision between two particles. We begin with a linear elastic model, and move on next to discuss the nonlinear elastic regime.[7]

Linear Model of a Binary Collision

We start with the simple case of two spheres colliding head-on, i.e., along a line joining their centers. If the distance between the surfaces of two particles of index i and j is denoted x, the differential equation governing x reads

$$\frac{d^2x}{dt^2} = \frac{f^{(i)}}{m_i} - \frac{f^{(j)}}{m_j},$$

where $f^{(i)} = f_{el}^{(i)} + f_n^{(i)}$, since only the normal force comes into play in a head-on collision. For simplicity, the vector notation has been dropped. The previous equation applies only when $x = \frac{1}{2}(d_i + d_j) - r_{ij} > 0$. Under these conditions, we have

$$\frac{d^2x}{dt^2} + \mu\frac{dx}{dt} + \omega_0^2 x = 0, \qquad (6\text{-}9)$$

[7]So as to limit ourselves to these regimes, we will refrain from discussing the simulations done by Taguchi, who added to the equations a viscous dissipative term [105], [106].

where μ is a coefficient describing a dissipative term introduced earlier in (6-7). Here we have $\mu = D_n$ and $\omega_0 = \sqrt{K/m_{ij}}$, where, as usual, m_{ij} is the reduced mass of the system of two particles. We immediately recognize the equation of a dampened harmonic oscillator, whose well-known solution is

$$x(t) = \frac{v_0}{\tilde{\omega}} e^{-\mu t} \sin(\tilde{\omega} t), \qquad (6\text{-}10)$$

where v_0 is the relative velocity just before the collision, and $\tilde{\omega}$ is the frequency of the dampened oscillation, with $\tilde{\omega} = \sqrt{\omega_0^2 - \mu^2}$. The rate at which the distance x varies is given by

$$\frac{dx}{dt} = \frac{v_0}{\tilde{\omega}} e^{-\mu t}[-\mu \sin(\tilde{\omega} t) + \tilde{\omega} \cos(\tilde{\omega} t)]. \qquad (6\text{-}11)$$

The duration t_c of the contact is provided by the expression

$$t_c = \frac{\pi}{\tilde{\omega}} = \frac{\pi}{\sqrt{(K/m) - (D/m)^2}}.$$

Contact ends when $x(t_c)$ becomes negative. Note that in the present model, t_c is independent of the relative velocity of the particles. We may define the equivalent of the coefficient of restitution ε introduced in Section 2.2.2 by writing

$$\varepsilon = -\frac{[dx/dt]_{t=t_c}}{[dx/dt]_{t=0}},$$

which leads to

$$\varepsilon = \exp\left(-\frac{\pi\mu}{\tilde{\omega}}\right) = \exp\left(-\frac{D}{2m} t_c\right).$$

This last relation clearly demonstrates the link between the loss of momentum during collision and the dissipative term D_n (or μ). The coefficient of restitution also turns out to be independent of the relative velocity.

We are now in a position to calculate the maximum penetration depth $x_{\max}$ along the same line we followed for Hertz's model (Section 2.2.2). Maximum penetration is obtained when the penetration velocity dx/dt vanishes at time $t = t_{\max}$. From (6-10) and (6-11), the result is

$$x_{\max} = \frac{v_0}{\tilde{\omega}} e^{-\mu t_{\max}} \sin(\tilde{\omega} t_{\max}) = \frac{v_0}{\omega_0} e^{-\mu/\tilde{\omega}} \sin^{-1}\left(\frac{\tilde{\omega}}{\omega_0}\right).$$

If the system is only slightly dissipative (for instance, when $\varepsilon \geq 0.9$), then $\omega_0 \gg \mu$, and $t_{\max}$ approaches the value $2t_c$, as in the case of Hertz's model. Under these circumstances, $x_{\max}$ reduces to

$$x_{\max} = \frac{v_0}{\omega_0}.$$

In other words, the penetration depth is then proportional to the relative velocity of the colliding particles. This result differs significantly from Hertz's model, which

predicts a much weaker dependence (as $v_0^{-1/5}$). We thus arrive at the conclusion that a linear elastic model deviates substantially from the physical behavior of real collisions.[8] It seems necessary to devise a more realistic model incorporating the nonlinear nature of the contact interactions. That is the objective of the next paragraph.

Nonlinear Model of a Binary Collision

Using the same notation as previously, we write a generalized form of the differential equation (6-9)

$$\frac{d^2x}{dt^2} + 2\mu x\left(\frac{dx}{dt}\right)^{\gamma} + \omega_0^2 x^{1+\beta} = 0,$$

which may be rewritten in a more standard form [60]

$$m\frac{d^2x}{dt^2} + \eta d\left(\frac{x}{d}\right)^{\gamma}\frac{dx}{dt} + Ed\left(\frac{x}{\beta}\right)^{\beta} x = 0, \tag{6-12}$$

where E depends on Young's modulus and Poisson's coefficient of the material, and η depends on the compression as well as the viscosity with respect to shearing. We note in passing that the dissipative term in this last equation corresponds to a purely viscoelastic interaction. As such, the equation does not account for plastic deformations, permanent distortions, or dissipation of vibrational excitations via phonons, all of which were mentioned during our discussion of Hertz's model in Section 2.2.2.

It is informative to consider a few particular cases in terms of values of the exponents β and γ:

(1) $\beta = 0$ and $\gamma = 0$ corresponds to the linear interaction described by (6-9).
(2) $\beta = \frac{1}{2}$ and $\gamma = 0$ corresponds to the situation described by Hertz's equation. This can be verified as an exercise.
(3) $\beta = \frac{1}{2}$ and $\gamma = \frac{1}{2}$ corresponds to a generalized situation (Kuwabara and Kono model) in which a viscoelastic compression is added to the normal elastic interaction [107]. In this model, the nonlinearity stems from purely geometrical properties of the penetration.

It should be fairly evident by now that modeling collisions between particles is not easy. The physics of contact interactions is inherently complex and remains poorly elucidated. Furthermore, good numerical algorithms are tricky to develop, because they have to scrupulously take into account all the time constants involved (such as the duration of collisions, the relative velocities, the time of free flights, and others). Carelessness is likely to lead to unphysical results. To illustrate the point, we proceed to discuss a completely artificial effect that comes up in models based

[8] We might come to the erroneous conclusion that the present simple model, based on coupled spring and dampener, is useless. In fact, it can be shown that, as long as the contact duration t_c is chosen judiciously, in other words, realistically from the standpoint of the physics of the materials involved, MD simulations yield results that turn out to be fairly satisfactory.

on soft spheres [60]. It has come to be known as the "detachment effect," because it causes an unphysical separation of particles undergoing multiple collisions. It can best be understood by pursuing the simple model used in Section 3.2.1 to describe the behavior of a one-dimensional stack of spheres subjected to a vertical sinusoidal excitation.

The Detachment Effect

This effect comes up in both one- and multidimensional configurations. It results from certain limitations of numerical simulations in hard-to-treat cases when the separation between spheres is comparable to the penetration depth. In light of our comments about the LRV procedure (Section 6.2.2), it is not hard to predict that such situations may lead to erroneous numerical predictions. To highlight the difficulties involved, we define an effective coefficient of restitution ε_{eff}, consistent with Section 2.2.2, by means of the expression

$$\varepsilon_{\text{eff}} = \sqrt{\frac{E_f}{E_0}},$$

where E_0 and E_f are the initial and final kinetic energies (before and after the collision). It is important to choose a suitable variable to analyze this problem. Numerical simulations suggest that one such variable is the ratio $\sigma = s_0/(v_0 t_c)$, where s_0 is the initial distance separating the colliding particles. Figure 127 shows how ε_{eff} depends on σ. The trend indicated in the figure seems to be "universal" in

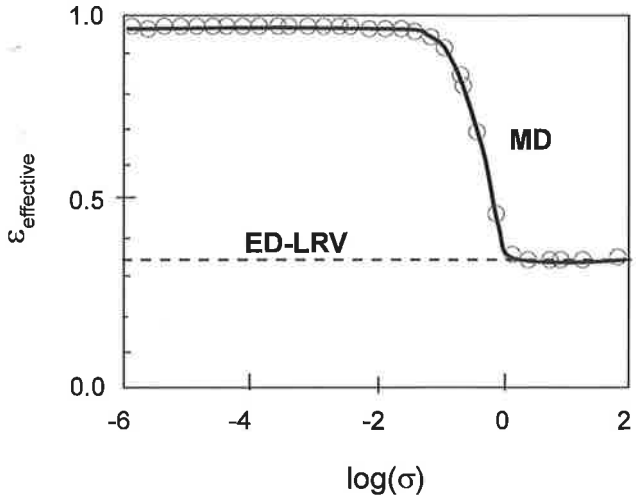

FIGURE 127. Effective restitution coefficient ε plotted against the ratio $s_0/v_0 t_c$ (see text). The horizontal line at $\varepsilon_{\text{eff}} \approx 0.34$ corresponds to the result of the ED–LRV procedure described in Section 6.2.2. The present results were obtained for a column of ten spheres and with fixed walls. The parameters used for the calculation were: $d = 1$ mm, $\varepsilon = 0.9$ (the true coefficient of restitution), $t_c = 0.0022$ s, and $v_0 = 0.03$ m/s (after [59]).

the sense that the results of MD simulations obtained for an extremely wide range of values of t_c (over three decades) and v_0 (varying by a factor of 400) all line up along the same curve.

The graph reveals a sudden change in the behavior of a column of spheres when $\sigma = 1$, that is to say, when the separation between particles becomes comparable to the distance traveled during the duration of a collision. As the separation becomes smaller than this critical value, the effective coefficient of restitution approaches unity. Such a result is in flagrant contradiction not only with experiments, but also with theoretical predictions that ε_{eff} should be a decreasing function of the number of particles. Here we find, instead, that it becomes equal to or larger than the coefficient of a single sphere, for which $\varepsilon = 0.9$. Put another way, the column appears far too "elastic," which from a practical point of view leads to an artificial separation of the colliding particles. No such problem exists when the initial separation is sufficiently large ($\sigma > 1$), in which case the molecular dynamics model agrees quite well with the results of the ED method. The latter technique, coupled with an LRV procedure, correctly predicts that ε_{eff} does not depend on σ. The artificial decompaction just discussed is at the origin of the designation "detachment effect," whose meaning is further illustrated in Figure 128.

Here the effect is clearly demonstrated when the particles are initially in contact. If we were to repeat the same calculations with particles initially separated by about 0.01 mm, the two techniques would produce virtually identical results.

There is, incidentally, another related phenomenon, known as the *brake failure effect*, when particles collide tangentially [108]. It comes about for very much the same reason. Here again, particles are slowed down considerably less in MD simulations than in other, more realistic, mechanics-based models.

We conclude this brief review of molecular–dynamics models with a more general remark, which in fact applies to all other simulation techniques as well.

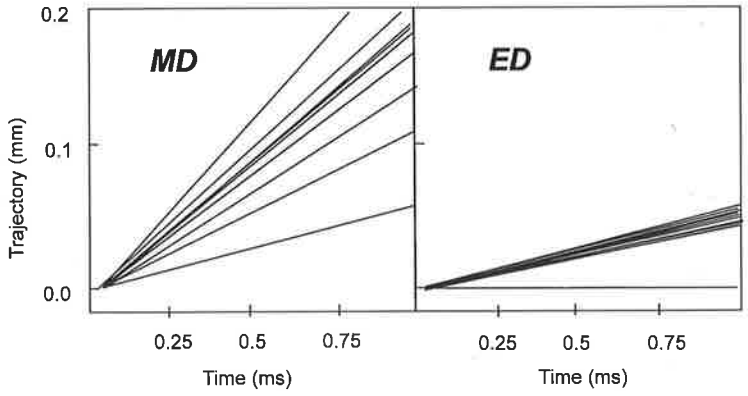

FIGURE 128. Trajectories of the centers of ten spherical particles. The MD model was carried out using exponents $\beta = \frac{1}{2}$ and $\gamma = 0$ (Hertz's model). Other parameters were: $\varepsilon = 0.86$, and $t_c = 6 \times 10^{-6}$ s for a binary collision, $v_0 = -0.2$ m/s, and $s_0 = 0$. The ED model used the same values (after [59]).

The results generally converge as long as the colliding particles spend most of their time sufficiently far apart, in which case the dynamic behavior of the entire system can be accurately modeled by a series of binary collisions. As soon as more than two particles come in contact at the same time, several questions come up. Are the collisions binary or ternary, or worse? Are we dealing with blocks? The answers are never simple, even from a straight physics point of view. All simulation techniques pay a price for this fundamental indeterminacy, although the symptoms may differ in each case. These difficulties manifest themselves in the form of inelastic collapse in ED models, or the detachment effect in their MD counterparts. As we pointed out in Section 3.1.1, short of knowing the details of interactions on a microscopic scale, we find ourselves rather helpless when it comes to predicting the dynamical behavior of a simple stack of as few as three particles when they are *almost in contact.*

6.4. Simulation of the Dynamics of Contacts

Fueled by a number of advances and remarkable successes, this technique is currently enjoying increasing popularity [109], [110]. It is rooted in basic research work on the mechanical properties of contacts. As we have emphasized repeatedly, the physics of granular materials is essentially governed by the mechanical properties of contacts. The merit of the technique we are about to present is to incorporate, as accurately as possible, a description of the various interactions between solids, consistent with the picture developed in Chapter 2. ED and MD methods are inherently dynamic in nature, and as such, they are ill-equipped to deal with prolonged contacts; indeed, they are essentially useless for modeling the static properties of granular piles. This points to the need for improved models. As noted in previous chapters, solid friction introduces not only an indeterminancy in the forces of contact (Section 3.1.1), but also complex stick–slip phenomena, all of which can be traced to the discontinuous nature of the forces involved when two solids in contact are displaced tangentially. By all indications, these discontinuities should play a critical role in the dynamic properties of granular materials.

Unfortunately, precisely because these forces are discontinuous, it is virtually impossible to write down an expression of the type $T = f(v_t, \gamma_t)$ that describes how the tangential friction force depends on the velocity and acceleration of the objects in contact (v_t and γ_t are the tangential velocities and accelerations, respectively). That is, of course, a major obstacle to devising an exact numerical treatment of the problem. Faced with this challenge, a number of researchers have proposed ways to "tame" the laws of contact, as it were. The underlying idea is illustrated in Figure 129.

It is useful to examine in more detail the nature of these irregularities. We distinguish three possible situations:

- As we know, the law of dry friction exhibits a discontinuity—more precisely, an indeterminacy if we do not know the past history of the contact—when

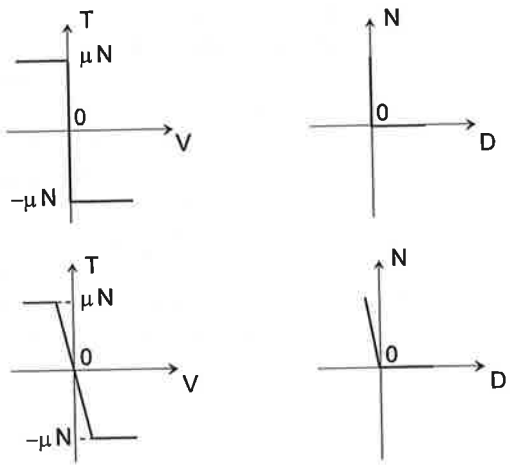

FIGURE 129. The diagrams on the left correspond to Coulomb's law of dry friction. T and N are tangential and normal forces. The diagrams on the right show Signorini's conditions. D is the distance between contact points. Both upper diagrams are discontinuous. The discontinuities have been partly mitigated in the lower figures. The gentler form of Coulomb's law implies a viscous interaction in the vicinity of the contact, while that corresponding to Signorini's condition assumes an elastic reaction when the solids get close to each other (after [111]).

the tangential velocity at the point of contact is zero. In this case, $v_t = 0$ and $\gamma_t = 0$, and the tangential resistance force can take on any value between $-\mu_s N$ and $+\mu_s N$. The contact forces are not activated. Static friction exactly offsets all other forces applied to the contact, preserving the condition $\gamma_t = 0$.

- If a sufficiently large tangential force is applied, the contact gives way ($\gamma_t \neq 0$). The equality $T = -\mu_s N$ sign (γ_t) holds, even just before motion actually begins (i.e., when we still have $v_t = 0$). In this situation, the forces of contact are fully activated.
- The contact is said to be *gliding* when $v_t \neq 0$, in which case $T = -\mu_d N$ sign (v_t).

A similar analysis can be done on the basis of Signorini's conditions, which deal with the normal, rather than tangential, forces. They apply to hard objects, considered impenetrable in the sense defined earlier:

- When $v_n = \gamma_n = 0$, the normal force opposing penetration can have any value $N \geq 0$.
- Contact is broken the moment $v_n = 0$ and $\gamma_n > 0$, in which case the normal force N must vanish.

From this point of view, Signorini's conditions exhibit very much the same type of discontinuity as Coulomb's law.

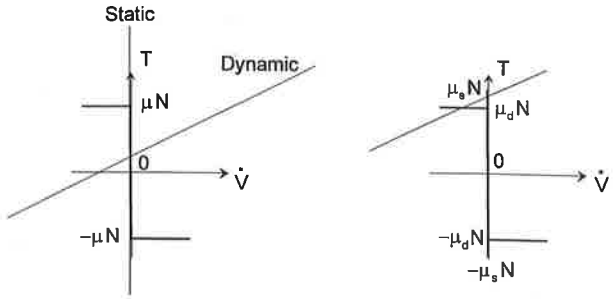

FIGURE 130. Schematic interpretation of the indeterminacies concerning the friction forces (after [111]).

An interesting exercise is to try to rederive the indeterminacies mentioned earlier on the basis of the above diagrams.[9] The fundamental equations of the dynamics of a system of two particles of reduced mass m_{red} in contact can be written (in projection on the principal axes at the contact point) as[10]

$$N = m_{\text{red}}\gamma_n + \Phi_n$$

and

$$T = m_{\text{red}}\gamma_t + \Phi_t,$$

where Φ_t and Φ_n are the normal and tangential components of the reaction force due to friction. These components depend on the mode of contact between the two particles, but not on the external forces, since we deliberately treat the two separately. If we work in the frame of reference attached to the contact point between the two particles, the fundamental equations are represented in the above diagrams by straight lines with a positive slope. These straight lines would intersect the discontinuous curves at a single point, as shown in Figure 130, which implies a unique solution. The problem is somewhat more complicated in the case of dry friction. Whether the solution is unique or not depends on the experimental conditions and the way Coulomb's friction is modeled. Figure 130 reveals the following:

- If dry friction is modeled with a single coefficient $\mu = \mu_s = \mu_d$, the solution is always unique for a dynamic interaction.
- For a static interaction, the straight line describing the fundamental equation becomes vertical, and the solution becomes undetermined (with an infinity of solutions).

[9] An excellent analysis of these indeterminacies and how to handle them mathematically can be found in [111].

[10] Here we neglect any possible rotation of the particles. It could easily be added to the equations, but it would not materially change the argument.

- If dry friction is modeled with two different friction coefficients μ_s and μ_d, with $\mu_s > \mu_d$, the straight line can intersect Coulomb's graph at two distinct points, and the solution is obviously not unique. Which solution the system chooses depends on its prior history, which opens the door to the kinds of hysteresis effects discussed in Sections 2.3 and 3.1.1. That is a commonly recognized characteristic studied in structural analysis [112].

These considerations may well elicit growing skepticism that it will ever be possible to accurately model any granular system that is subject to such intrinsic indeterminacies. As we now know, these indeterminacies all come from the discontinuous character of the static resistance force. One way to get around this problem is to resort to well-behaved functional dependences of the type depicted in the lower part of Figure 129. Another way is to consider the static situation simply as a limiting case of the dynamic problem (when $v \to 0$). Such arguments may indeed be viewed as a posteriori justifications of the MD and ED simulations techniques which, being inherently dynamical approaches, avoid these problems entirely. It is also essential to bear in mind that we have considered only hard objects (in the sense of the hard spheres in ED simulations). The creation and rupture of micro-contacts is unlikely to be as discontinuous as implied by the standard constitutive laws. It is in fact quite plausible that smoother functions might describe real phenomena more realistically. What we can say with some confidence is that various models based on the arguments presented above generally lead to results in good agreement with experiments [111]. This includes ED and MD simulations, as well as others to be discussed in the latter part of this chapter. There is no compelling reason to promote any one technique over another. In all likelihood, a particular approach, based on specific simplifying assumptions, can be perfectly adequate in certain circumstances, and completely break down in others. The best strategy is to be flexible and keep an open mind.

We proceed next to discuss two more simulation techniques, based on procedures for synthesizing piles. These methods may appear somewhat primitive when compared to the ones reviewed thus far. Yet, they too turn out to produce very satisfactory results, at least when the geometry of a pile is an important factor.

6.5. Monte Carlo (MC) Simulations

There exists an extensive literature on the topic of Monte Carlo simulations. It is not our purpose here to offer a comprehensive analysis of the technique, which has been used to solve a great many problems in statistical mechanics, among other applications. Instead, we will highlight its ability to provide numerical solutions to some important problems in the physics of granular materials. We will do so by using the celebrated example of the "Brazil nut problem" [88], [92], [113]. As discussed in Section 5.2, it involves the phenomenon of segregation by size. We will later on introduce a rather different approach, known as the *method of steepest descent*, which has also proven very useful.

We start by emphasizing the *sequential character* of the stacking method used by both methods. Time is managed in both cases by providing for a relaxation phase between successive stages of building up the stack. In that sense, we are dealing here with a truly sequential procedure of the type we described in connection with the SOC cellular automation model (Section 4.2.1). The chain of events can be represented symbolically by

$$\textit{preparation} \Rightarrow \textit{relaxation} \Rightarrow \textit{stacking} \Rightarrow \textit{relaxation} \Rightarrow \textit{etc.}$$

Let T be one period of the stacking–relaxation cycle. It is worthwhile to pause a moment to understand the implications and limitations of this strategy, in the light of what we have learned in previous chapters about collision models and the behavior of granular piles. First of all, this procedure obviously overlooks the dynamical properties of collisions. Barring additional refinements, it ignores all the problems associated with solid frictional dissipation, whether static or dynamic. Accordingly, we should not expect this approach to properly describe the behavior of a collection of particles in frequent collisions. To be more specific, we designate by τ_1 the time interval between the two closest sequential events defining the dynamics of the pile. In the language of ED modeling of a vibrated one-dimensional stack (Section 3.2.1), τ_1 would be the time between two successive collisions. As we have seen, this time can become infinitesimally small, giving rise to what is known as "inelastic collapse." Under these same circumstances, tracking the evolution of the system with an MD method would require sampling with a period $T < \tau_1$, which could easily entail prohibitive computational times. Short of that, the subtle details of the mechanics of systems undergoing multiple collisions would be at risk of being missed. This would be equivalent to neglecting events on a short spatial scale λ (of the order of the distance separating particles), which could lead to erroneous results. The Monte Carlo method specifically deals with successive states of a granular medium *after it has relaxed.* As such, it is particularly well suited to describing the physics of granular objects over fairly long time intervals, such as when they are excited periodically and sufficiently slowly to leave enough time for the pile to relax between successive excitations.[11] With these precautions in mind, the stacking techniques discussed here can be extremely valuable, notably for the purpose of analyzing the phenomenon of segregation by size [113]. The next paragraph outlines the practical steps required to implement a Monte Carlo simulation.

Monte Carlo Technique for Stacking and Relaxation

The methodology described here was originally used in numerical simulations of the Brazil nut problem [88], [113]. It subsequently benefited from a number of improvements which led to results in perfect agreement with the topological models discussed in Section 5.2.1 [92]. For pedagogical purposes, we will begin

[11] It might be worthwhile to reread the portion of Section 3.2.1 dealing with the excitation period T in relation to the relaxation time τ of the system. We can also appreciate that the MC method should be applied preferably to materials with a low coefficient of elastic restitution ε, simply because the relaxation following excitation is typically a fairly rapid phenomenon.

by following fairly closely the traditional way of using Monte Carlo calculations. We will subsequently discuss the specifics of applying the technique to granular materials.

Although we could, without unduly complicating the problem, treat the case of a three-dimensional pile of dissimilar granules, we consider, instead, a collection of identical disks of diameter d. These disks, assumed to be impenetrable, are initially arranged randomly in a hypothetical vertical two-dimensional container without walls.[12] In practice, this is approximated by using a ring-shaped container. The initial configuration of such a system of N disks is described by a generalized vector encompassing the coordinates of all centers

$$\tilde{r} = \{r_1, r_2, r_3, \ldots, r_N\}.$$

The potential energy $E_g(\tilde{r})$ of the system is given by

$$E_g(\tilde{r}) = \sum_{j=1}^{N} mgz_j, \tag{6-13}$$

where m is the mass of an individual disk and z_j is the altitude of its center. The Monte Carlo method is based on analyzing the probability P of different configurations $\tilde{r}$, each of which has an energy $E_g(\tilde{r})$. Thermodynamics tells us that

$$P[E_g(\tilde{r})] = \frac{1}{Q}\exp\left[-\frac{E_g(\tilde{r})}{kT}\right],$$

where Q is the partition function of the system, and T is its absolute temperature. Note that this last expression characterizes all the configurations that are equivalent from an energy point of view, in equilibrium at temperature T. They only differ by the actual positions of the individual disks.

The technique consists in examining the probabilities of all possible configurations arrived at by moving every disk in the population within a small region of area δ^2. We write this process as a set of equations

$$x_j' = x_j + \xi_x\delta \tag{6-14a}$$

and

$$z_j' = z_j + \xi_z\delta, \tag{6-14b}$$

where ξ_x and ξ_z are independent random variables equally distributed in the interval $[-1, +1]$, and $\delta > 0$. So as to ensure that the disks do not penetrate each other during the successive trials, we require that the interaction between adjacent particles be governed by a potential energy $U(s)$ of a pair such that

$$U(s) = 0 \qquad \text{if} \quad s \geq d \tag{6-15a}$$

[12] This is a crucial restriction. We have seen in Chapters 3 and 5 that walls induce convection effects in granular media. By getting rid of them, convection is conveniently eliminated. All that is then left are geometrical phenomena, such as "arch effects" of the type described in Section 5.2.1.

and

$$U(s) = \infty \qquad \text{if} \quad s < d. \tag{6-15b}$$

The trials conducted according to (6-13) through (6-15) must be evaluated for plausibility against the following criteria:

- If the quantity

$$\Delta E = E(\tilde{r}') - E(\tilde{r}) \leq 0, \tag{6-16}$$

  the new configuration has a lower energy than the one we started with. It is therefore retained for subsequent calculations.
- If $\Delta E > 0$, the solution $\tilde{r}$ is not necessarily rejected, as it may well be accessible via simple thermal agitation. It is therefore assigned a probability given by

$$P(\Delta E) = \frac{P[E(\tilde{r}')]}{P[E(\tilde{r})]}\exp\left(-\frac{\Delta E}{kT}\right). \tag{6-17}$$

  In turn, this probability is compared to a random number ξ uniformly distributed between 0 and 1. If $P(\Delta E) \geq \xi$, the solution is retained. If not, it is discarded, and another one is tried.

The procedure calls for jiggling every single particle of the system, until each member of the population has had its turn, which completes one iteration. The new configuration is then used as a fresh starting point for the next iteration, in which all particles are moved about all over again and allowed to relax, and so forth.

Some comments on the temperature of the system are in order. The method we have just described is essentially what is used traditionally for Monte Carlo simulations of Brownian systems. When it is applied to macroscopic objects like granular materials, the significance of equations involving the thermal energy kT raises some legitimate questions.

As pointed out in Chapter 1, the Brownian motion of typical systems of interest here is entirely negligible, the ratio $mg\Delta z/kT$ being of the order of 10^{12} at ordinary temperatures. If so, (6-17), and the criterion associated with it, gives a probability that is always practically zero. In other words, the only really relevant equation for a granular system is (6-16), which means that the potential energy can only decrease at each step of the iteration. This is equivalent to assuming that the temperature of the system is at absolute zero. The clear implication is that the system traps particles in potential wells from which they cannot escape without collisions on a microscopic level. In accordance with our earlier discussions, it is clear that this simulation strategy amounts to neglecting the short-range interactions normally associated with multiple collisions—which are equivalent to a local temperature of the granular. Rather, it deals fundamentally with systems in their relaxed states.

Despite these restrictions, this type of simulation technique has proven extremely useful to model a number of situations, such as a pile of dissimilar particles. By way of summary, we emphasize again that, by its very nature, this particular technique is not a good choice to describe nonrelaxed configurations, where particles spend only a fraction of their time in actual contact. One important example is that of fluidized beds, which are more suitably treated by ED or MD simulations.

6.6. Sequential Model of a Pile

Monte Carlo simulations were based on keeping track of the energy of the various geometrical configurations a pile of N particles can find itself in. The system evolved from an initial state of energy $E(\tilde{r})$ to a final state of energy $E(\tilde{r}')$, with $E(\tilde{r}') < E(\tilde{r})$, without us having to worry at all about the details of the relaxation process. Another strategy would be to mimic as realistically as possible the local mechanical properties of the system. That is precisely the idea behind the so-called method of *steepest descent* [91].

The principle of the technique is illustrated in Figure 131. The objective is to model the way particles fall down on top of each other. The algorithm can be summarized as follows:

- Spherical particles are dropped sequentially on top of the forming pile in a random manner, in the sense that the coordinate x where they are deposited is a random variable, as described in [114].
- After a particle is dropped at a random spot, it follows a "natural" downward slope, along a path described as the *steepest descent*, until it finds a position of local equilibrium. Such a position, marked "stop" in Figure 131, occurs when the vertical projection of the particle's center crosses the line connecting

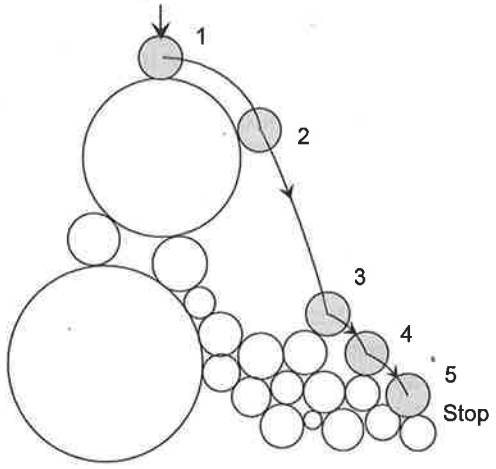

FIGURE 131. Illustration of the method of steepest descent (after [116]).

the centers of the two underlying particles. We note, incidentally, that this assumes the absence of any rebound when the particle raches that favorable spot, in accordance with earlier remarks on these stacking methods.

- Once a particle stops, it becomes permanently embedded in the pile.

Agitation can be simulated, for instance, by perturbing the entire system upward and leaving it to relax on its own. This can be accomplished in the following manner:

(1) A pile is first generated, by randomly depositing particles one at a time and allowing them to relax after each addition, using the algorithm just described.
(2) The stacked particles are numbered in ascending order starting from the bottom.
(3) The entire pile is raised (fictitiously), and each particle is left to fall down individually, again using the above algorithm. The process starts with the lowest-numbered particles and gradually works its way up. To some extent, it preserves a memory of the pile's prior configuration.[13]
(4) Steps (2) and (3) are repeated many times, thereby simulating a vertical vibration.

This type of simulation is relatively frugal in terms of computation time. It is the technique of choice to treat cases involving large numbers of particles in three dimensions. However, the limitations discussed in the context of the Monte Carlo method apply here as well. Both techniques are good choices to treat a series of relaxed states, to the specific exclusion of rapid interactions and multiple collisions that may occur in real systems. The method of steepest descent is particularly well suited to dealing with problems in which geometry is of paramount importance. It has produced results in relatively good agreement with experiments. Perhaps its greatest claim to fame is to have predicted the existence of critical diameters in the Brazil nut problem, similar to the ones we found analytically in Section 5.2.1.[14]

[13] We encourage the reader to refresh his or her memory by going back to the part of Chapter 3 that describes the various modes of decompaction of a pile under vertical excitation, particularly in one and two dimensions. This will provide further opportunities to reflect on the degree of realism of the present algorithm.

[14] The algorithm described here was originally developed by Jullien et al. [91]. Interestingly, early versions did not include noise, that is to say, random fluctuations of the particles's positions during the stacking of the pile, making it entirely deterministic. One consequence was that segregation was precluded for $\Phi < \Phi_c$, whereas the analytical model in Section 5.2.1 predicts merely a change in behavior as the critical value Φ_c is crossed. A noise source was subsequently added to the model, and a more realistic behavior did indeed result from this improvement.